



# Diffusion Welding for TC4 Titanium Alloy/T2 Copper with Vanadium Foil

TC4 titanium alloy and T2 copper were welded by vacuum diffusion with vanadium as an interlayer to explore the influence of temperature and time

BY B. WU, H. DONG, Y. MA, P. LI, C. LI, L. HUANG, AND L. ZHANG

## Abstract

TC4 titanium alloy (TC4) was vacuum diffusion welded to T2 copper (T2) with vanadium (V) foil as an interlayer. The influence of process parameters on elemental diffusion behavior, microstructure evolution, and shear performance of welded joints was explored. An obvious solid-solution diffusion zone appeared in the welded interface between TC4 and V, but no distinct diffusion zone formed in the joint interface of V/T2. The solid-solution phases of  $(Ti_6, V)_{ss}$ ,  $(Ti_3, V)_{ss}$ , and  $(Ti, V_7)_{ss}$  appeared in the interface of TC4/V. The crystallographic orientations of  $(Ti_6, V)_{ss}$ ,  $(Ti_3, V)_{ss}$ , and  $(Ti, V_7)_{ss}$  phases in high-resolution transmission electron microscope images were (002), (201), and (121), respectively. The lattice mismatch between  $(Ti_6, V)_{ss}$  and  $(Ti_3, V)_{ss}$  was calculated to be 11.9%. The activation energy to form a stable solid solution between titanium and vanadium was 226.6 kJ/mol. The highest shear strength of the welded joint reached 160 MPa, obtained at 860°C (1580°F) for 60 min. The joint fractured along the interface of V/T2, illustrating that the solid-solution structure between Ti and V was stronger than the metallurgical bonding between V and Cu. The fracture surface of the welded joints revealed a river pattern and ladder topography, representing a cleavage fracture mode. FCC-Cu, BCC-V, and  $\beta$ -Ti were detected on both fracture surfaces of the TC4 titanium alloy and T2 pure copper sides. The influence of welding temperature on the diffusion of V in Ti was greater than on Ti in V, and Ti and Cu diffused faster than V in the joint.

## Keywords

- Dissimilar Materials
- Vacuum Diffusion Welding
- Vanadium Interlayer
- Interfacial Microstructure
- Diffusion Mechanism
- Mechanical Performance

## Introduction

More attention has been paid to joining dissimilar materials because it can make full use of the advantages of dissimilar materials to meet the requirements of structure and performance (Refs. 1–5). The linear thermal expansion coefficient, thermal conductivity, atomic radius, and lattice constant between dissimilar materials are various (Refs. 6–8). Therefore, it is extremely difficult to effectively join dissimilar materials using traditional fusion welding processes (Ref. 9). Diffusion welding, a superior solid-state welding method, has been applied to weld most similar and dissimilar materials (Refs. 10–12). Plastic deformation and atomic diffusion occur during diffusion welding, then a diffusion layer forms at the joining interface that achieves a reliable connection. The key factors for diffusion welding include welding temperature, holding time, pressure, surface roughness, and interlayer composition (Refs. 13, 14).

However, if directly welded, dissimilar materials joints could produce many harmful intermetallic compounds (IMCs) and residual stress, reducing their mechanical properties. Titanium and titanium alloys have been extensively used in the aerospace, electrical and electronics, and biomedical engineering fields because of their specific strength, low thermal elasticity, superior low-temperature performance, and corrosion resistance (Refs. 15–17). Copper and copper alloys are widely applied in the electrical appliances, shipping, and nuclear power fields due to their advantages, such as excellent electrical and thermal conductivity, high-oxidation resistance, and excellent cold and hot working performance (Refs. 18, 19). Especially, those remarkable comprehensive properties make it possible for hybrid structures of titanium and copper to be substitutions for steel and copper. The coefficients of linear expansion for T2 copper (T2) and TC4 titanium alloy (TC4) are correspondingly  $16.7 \times 10^{-6} K^{-1}$  and  $8.3 \times 10^{-6} K^{-1}$ . According to Aydin et al. (Ref. 20), various brittle  $Ti_xCu_y$  IMCs appeared at the welded interface of

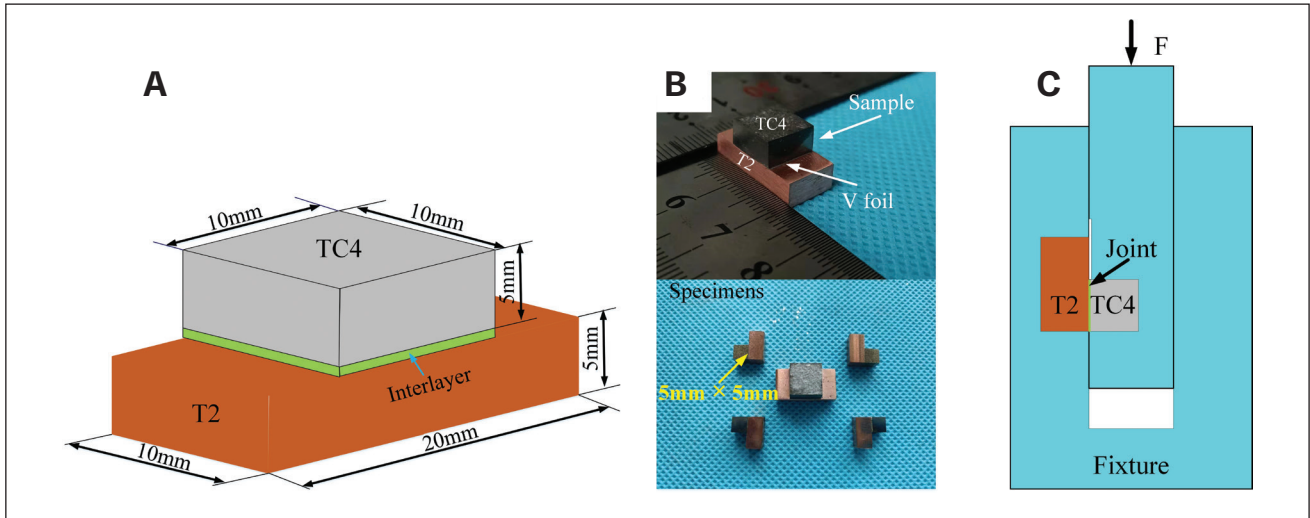


Fig. 1 – A – Assembly morphology of the samples with V foil; B – image of diffusion welded joint and cutting samples; C – shear test of the welded joint.

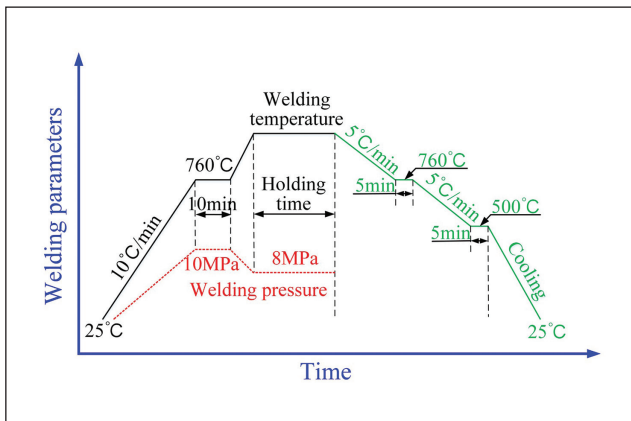


Fig. 2 – Process parameter curve of diffusion welding between TC4 and T2 with a V interlayer.

electrolytic copper to TC4 titanium alloy, decreasing the shear properties of the welded joint. Based on the Ti-Cu binary phase diagram, these IMCs mainly include the  $Ti_2Cu$ ,  $TiCu$ ,  $Ti_2Cu_3$ ,  $Ti_3Cu_4$ , and  $TiCu_2$  phases at the temperature range of  $700^\circ\text{C} \sim 900^\circ\text{C}$  ( $1292^\circ\text{F} \sim 1652^\circ\text{F}$ ) (Ref. 21). Therefore, it is important to use a proper interlayer to reduce or eliminate these IMCs caused by the differences in the chemical and physical performances of dissimilar materials.

Nevertheless, vacuum diffusion welding between titanium and copper has had limited revelations in literature. Shen et al. (Refs. 22, 23) investigated diffusion welding of oxygen-free copper to TC4 titanium alloy with an OCr18Ni9 stainless steel interlayer and a pure Ag interlayer, respectively. Their results demonstrated that the interlayer could effectively prevent the appearance of harmful intermetallic compounds, and the tensile property of the welded joint was improved by more than 140 MPa. Zhao et al. (Ref. 24) reported diffusion welding between ZQSn10-10 alloy and TC4 titanium alloy using Ni/Cu multi-interlayers. The optimum tensile strength

of the joint reached 155.8 MPa, which is equivalent to 65% of ZQSn10-10 alloy. Thus, a proper interlayer can improve the microstructure and properties for the resultant joints.

The element vanadium has many excellent physical and chemical properties, including excellent ductility, wear resistance, and nonmagnetic and corrosion resistance. In addition, adding vanadium can refine the microstructure and improve the mechanical properties of alloys. Therefore, it is known as the vitamin in metals. Vanadium is a stabilizer of the  $\beta$  phase in titanium alloys (Ref. 25). Based on the Ti-V binary phase diagram, a stable infinite solid solution can form between titanium and vanadium. The liquidus temperature between vanadium and copper is high and the solubility is low based on the V-Cu binary phase diagram. Therefore, vanadium hardly reacts with copper, and metallurgical bonding occurs only through atomic diffusion. In this paper, TC4 and T2 were welded by vacuum diffusion with vanadium as an interlayer. The influence of temperature and time on the microstructure evolution and shear properties of the resultant joints was explored.

## Experimental Methods

TC4 titanium alloy and T2 copper were welded by vacuum diffusion with 99.99% pure vanadium (V) foil as an interlayer. The chemical composition of the base materials and interlayer are listed in Table 1. The samples of TC4 and T2 were cut into sizes of  $10 \times 10 \times 5 \text{ mm}^3$  and  $20 \times 10 \times 5 \text{ mm}^3$  using a wire cutting machine. The thickness of vanadium foil is about  $70 \mu\text{m}$ . Before vacuum diffusion welding, these samples to be welded were polished with up to 2400 grit sandpaper and then eliminated by ultrasonic equipment to wipe off the oxide film. The surface roughness of the welded samples was measured by laser confocal microscopy to be about  $0.08 \mu\text{m}$ .

The specimens were assembled as displayed in Fig. 1A. This welding experiment proceeded in a ZTF2-10 vacuum

**Table 1 – Elemental Composition of Raw Materials and V Foil (wt-%)**

| Materials | Al   | V     | Fe   | O    | Si     | P      | S      | Ti   | Cu   |
|-----------|------|-------|------|------|--------|--------|--------|------|------|
| TC4       | 6.18 | 3.87  | 0.02 | 0.14 | —      | —      | —      | Bal. | —    |
| T2        | —    | —     | —    | —    | ≤ 0.04 | ≤ 0.02 | ≤ 0.02 | —    | Bal. |
| V foil    | —    | 99.99 | —    | —    | —      | —      | —      | —    | —    |

**Table 2 – Vacuum Diffusion Welding Process Parameters Applied in the Experiment**

| Welding Temperature (°C) | Holding Time (min) | Welding Pressure (MPa) |
|--------------------------|--------------------|------------------------|
| 840                      | 30                 | 8                      |
| 840                      | 45                 | 8                      |
| 840                      | 60                 | 8                      |
| 860                      | 30                 | 8                      |
| 860                      | 45                 | 8                      |
| 860                      | 60                 | 8                      |
| 880                      | 30                 | 8                      |
| 880                      | 45                 | 8                      |
| 880                      | 60                 | 8                      |

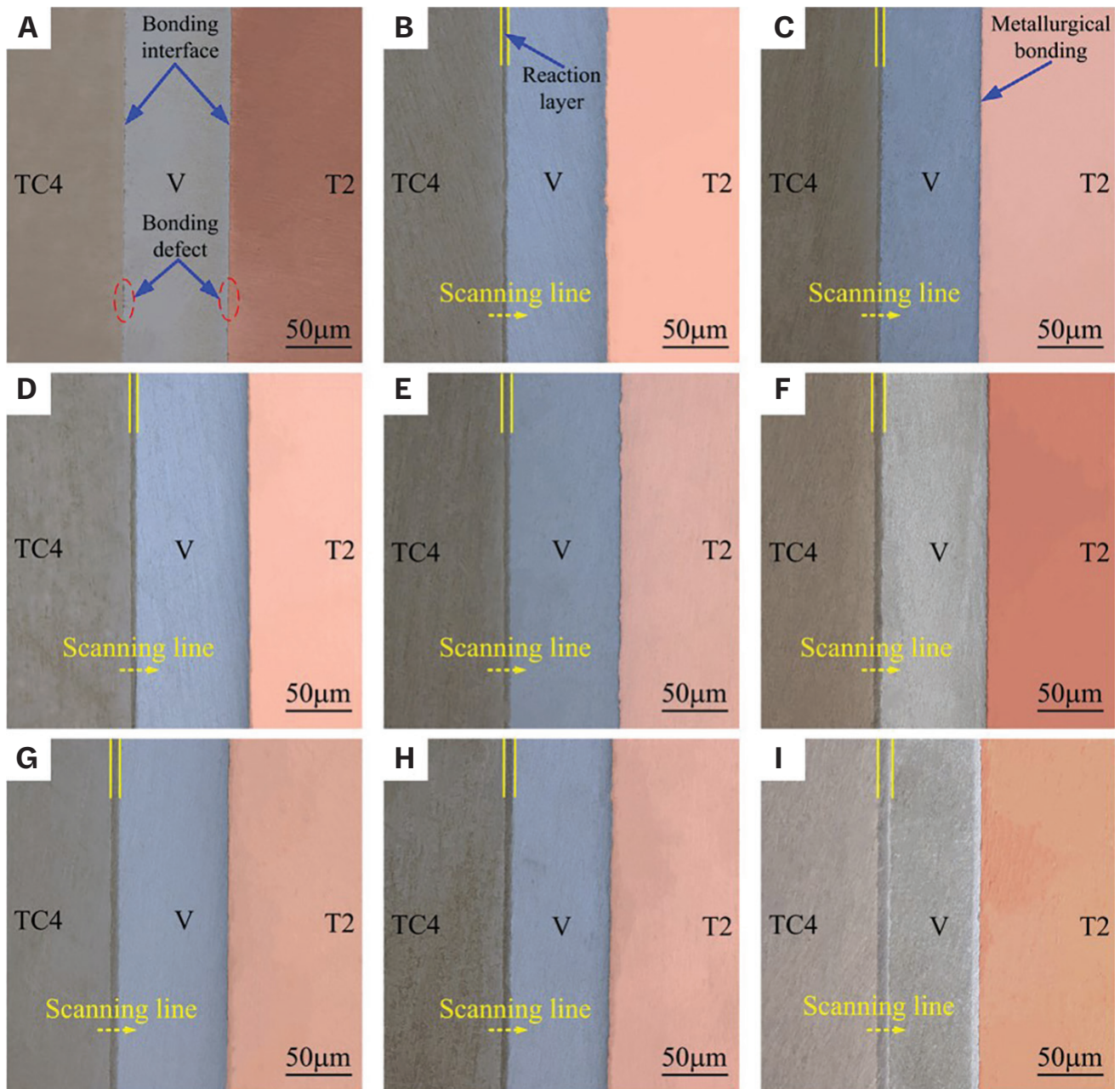


Fig. 3 – Macromorphology of joints under different parameters: A – 840°C/30 min; B – 840°C/45 min; C – 840°C/60 min; D – 860°C/30 min; E – 860°C/45 min; F – 860°C/60 min; G – 880°C/30 min; H – 880°C/45 min; I – 880°C/60 min.

diffusion welding furnace with a vacuum degree of  $3 \times 10^{-3}$  Pa. The photos of the diffusion welded joint and shear samples are shown in Fig. 1B, and the shear test of the welded joint is displayed in Fig. 1C.

In general, the theoretical welding temperature scope of diffusion welding is  $0.65T_m - 0.85T_m$  ( $T_m$  is the melting point for the materials to be welded) (Ref. 26). The melting points of T2 pure copper and TC4 titanium alloy are correspondingly 1080°C (1976°F) and 1667°C (3033°F). Therefore, the theoretical welding temperature scope is from 660°C (1220°F) to 860°C (1580°F). In addition, the high-

temperature yield performance of T2 pure copper is low: less than 10 MPa at 900°C. Therefore, the welding pressure was selected as 8 MPa to prevent a severe variant of T2. The temperatures of 840°C (1544°F), 860°C, and 880°C (1616°F) were selected during the vacuum diffusion welding of TC4 to T2 with V foil as the interlayer. According to a preliminary study (Ref. 27), the welding process was mainly split into two stages when the samples were heated. The process parameter curve of diffusion welding between TC4 and T2 with a V interlayer is shown in Fig. 2.

**Table 3 – Component Analysis Results of the Marked Points in Fig. 6 (at.-%)**

| Location | Ti    | Cu    | Al   | V     | Possible Phase                      |
|----------|-------|-------|------|-------|-------------------------------------|
| A        | 81.61 | —     | 4.83 | 13.48 | (Ti <sub>6</sub> V) <sub>ss</sub>   |
| B        | 68.99 | —     | 4.37 | 25.81 | (Ti <sub>3</sub> V) <sub>ss</sub>   |
| C        | 12.78 | —     | 0.31 | 86.29 | (Ti, V <sub>7</sub> ) <sub>ss</sub> |
| D        | —     | 86.08 | —    | 13.17 | FCC-Cu + BCC-V                      |
| E        | 82.46 | —     | 4.02 | 13.68 | (Ti <sub>6</sub> V) <sub>ss</sub>   |
| F        | 71.33 | —     | 4.08 | 24.12 | (Ti <sub>3</sub> V) <sub>ss</sub>   |
| G        | 13.13 | —     | 0.59 | 86.27 | (Ti, V <sub>7</sub> ) <sub>ss</sub> |
| H        | —     | 86.12 | —    | 13.88 | FCC-Cu + BCC-V                      |

The welding temperature enlarged from 25°C (77°F) to 760°C (1400°F) under the speed of 10°C/min (50°F/min) and then kept for 10 min, which could ensure the proper bearing contact of contact surfaces and wipe out the microscopic voids. Secondly, the samples were heated to the welding temperature and held for a period of time under 8 MPa of pressure. After welding was completed, the pressure was backout. Upon cooling, T2 seriously contracted due to the quick cooling rate, which easily led to the cracking of joints. Therefore, a process of slow heat treatment cooling was applied in this study. The vacuum diffusion welding parameters are shown in Table 2.

After diffusion welding was completed, the pressure shear experiment of the samples was examined by the DSN-200 testing machine at a speed of 1 mm/min. Three same-compression shear specimens were tested to acquire the medial shear performance of welded joints (Fig. 1B). The compression shear performance of the welded joint was obtained according to the following relation (Ref. 28):

$$\tau = \frac{P}{wl} \quad (1)$$

where  $P$  and  $\tau$  are the compression shear stress and compression-shear performance and  $w$  and  $l$  are, correspondingly, the height and length of the welded joint. In this

experiment,  $w$  and  $l$  were both 5 mm (0.2 in.) (Fig. 1B). After the shear test, the phase composition of the failed joint was measured through an x-ray diffractometer (XRD-Empyrean). The XRD experiment was operated using Cu radiation, and the voltage and current range were, correspondingly, 10–50 kV and 4–50 mA. A JSM-5600LV scanning electron microscope (SEM) equipped with an energy-dispersive spectrometer (EDS) was used to obtain the phase constituents. The voltage, resolution ratio, and spectral resolution for the JSM-5600LV SEM were, correspondingly, 15 kV, 3.4 nm and 132 ev. The macroscopic interfaces and fracture morphologies of the welded joints were examined by a laser confocal microscopy (OLS4000). The reaction phases were detected through a transmission electron microscope (TEM, JEOL JEM-2100F). The TEM sample was prepared by a focusing ion beam (FIB). The microstructure, quantitative point composition, and distribution of elements for the welded joint were analyzed through an electron probe microanalyzer (EPMA-1600).

## Results and Discussion

### Interfacial Microstructure

The macromorphology of joints under various parameters is exhibited in Fig. 3. Unbonded defects existed in the

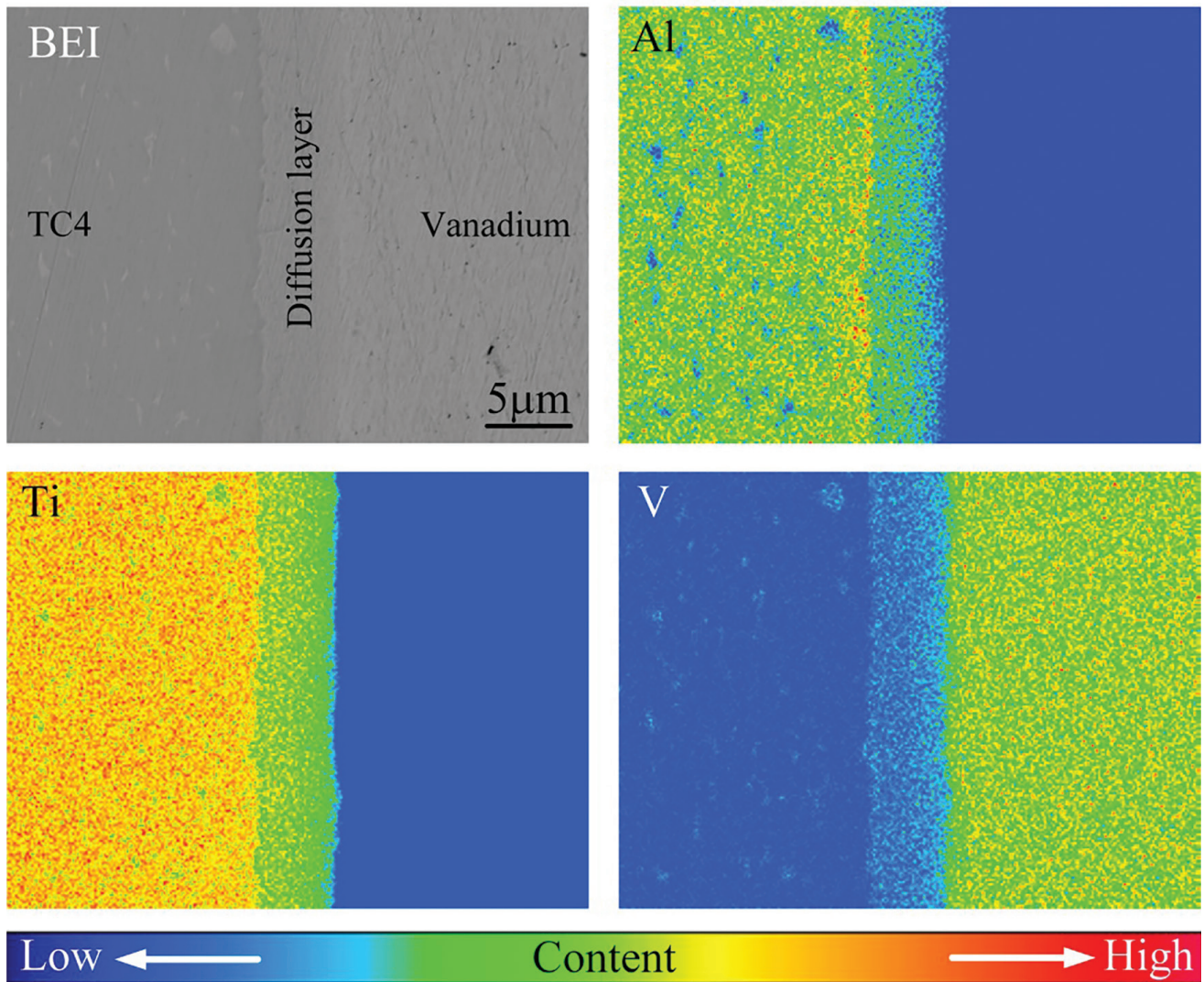


Fig. 4 – Elemental mapping results for the diffusion layer between TC4 and V at 860°C for 60 min.

TC4/V and V/T2 interfaces obtained at 840°C for 30 min due to low welding temperature and short diffusion time. The unwelded defect vanished with the increase of welding temperature and holding time. An apparent reaction zone appeared in the welded interface of TC4/V, while atomic diffusion occurred between V and T2, but no obvious diffusion zone appeared. The interfacial layer of TC4/V existed as a solid solution rather than an intermetallic compound due to similar chemical and physical performance. Moreover, the width of the diffusion zones between TC4 and V enlarged gradually with the increase of welding temperature and holding time (Fig. 3); however, this welding interface between V and T2 had no noticeable variation. The width of the reaction zone between TC4 and V was inhomogeneous when the welding temperature and time were below 860°C and 45 min, respectively. This was mainly attributed to the insufficient diffusion of atoms in the welded interface.

### Quantitative Analysis and Elemental Distribution

To further analyze the diffusion behavior of interface elements, map scanning of the welded joint was conducted by the EPMA. The mapping results of alloying elements in the diffusion layer between TC4 and V at 860°C for 60 min are listed in Fig. 4. Ti, V, and Al were uniformly distributed in the reaction zone, and the titanium concentration was higher than the vanadium concentration (Fig. 4). The concentration gradients of alloying elements were the driving force for the diffusion and diffusion welding. In addition, a small amount of the Al element was also distributed in the continuous solid-solution diffusion layer formed by the reaction between Ti and V. The concentration of the Al element in the solid solution near the TC4 side was higher than that near the T2 side, which was mainly caused by the different coefficients of self-diffusion and interdiffusion between alloying elements. The diffusion rate of V in Al was several orders of magnitude

**Table 4 — Average Thickness and Diffusion Coefficient for the Diffusion Zone of the TC4/V Interface**

| Bonding Temperature (°C) | Holding Time (min) | Average Thickness (μm) | Diffusion Coefficient (m <sup>2</sup> · s <sup>-1</sup> ) |
|--------------------------|--------------------|------------------------|---|
| 840                      | 30                 | —                      | —   |
| 840                      | 45                 | 3.2                    | 3.79 × 10 <sup>-15</sup>                                  |
| 840                      | 60                 | 3.7                    | 3.80 × 10 <sup>-15</sup>                                  |
| 860                      | 30                 | 3.9                    | 8.45 × 10 <sup>-15</sup>                                  |
| 860                      | 45                 | 4.9                    | 8.89 × 10 <sup>-15</sup>                                  |
| 860                      | 60                 | 5.6                    | 8.71 × 10 <sup>-15</sup>                                  |
| 880                      | 30                 | 6.5                    | 2.35 × 10 <sup>-14</sup>                                  |
| 880                      | 45                 | 7.5                    | 2.08 × 10 <sup>-14</sup>                                  |
| 880                      | 60                 | 9.3                    | 2.40 × 10 <sup>-14</sup>                                  |

faster than that of Al in V, as reported by Huang et al. (Ref. 29). Interfacial element diffusion is related to element concentration and enthalpy of mixing. The enthalpy of mixing for Al and V with Ti are correspondingly -2 and -16 kJ/mol (Ref. 30). The mixing enthalpy of elements is more negative, the diffusion reaction is more likely to occur, and then the continuous solid-solution diffusion layer will easily form in the interface. Huang et al. (Ref. 29) pointed out that the Ti element diffuses faster than Al when the Al content is less than 25 at.-%, and Ti is always the faster diffuser when the diffusion couple is in a concentration range. Therefore, the continuous solid-solution layer was formed in the interface of TC4/V due to the low content of the Al element in TC4. However, the concentration of V and Cu did not change significantly at the interface of V/T2. The distribution of V and Cu in the diffusion layer of V/T2 at 860°C for 60 min is displayed in Fig. 5. The interface of V/T2 had no obvious diffusion layer compared with the interface of TC4/V (Fig. 5). In addition, the welded interface of V/T2 was uneven, which was related to element diffusion between V and Cu. The mixing enthalpy

of V and Cu is 5 kJ/mol (Ref. 30), illustrating that atomic diffusion occurs between V and Cu instead of the chemical reaction. Therefore, the joining between V and Cu belongs to metallurgical bonding.

The analysis of point composition was applied to speculate these phases in the interface. Figure 6 shows the microstructure of the reaction zone under 840°C/45 min and 880°C/60 min. The EPMA quantitatively analytical data of the marked points in Figs. 6B, C, and F–H are listed in Table 3.

A distinct reaction zone formed at this interface of TC4/V, and there was a bright-white band and a couple of raised ridges near the V and TC4 sides, respectively (Figs. 6B, F). According to the element content in Table 3, the raised ridge (Location A), diffusion layer (Location B), and bright-white band phase (Location C) correspondingly may be solid-solution phases of (Ti<sub>6</sub>V)<sub>ss</sub>, (Ti<sub>3</sub>V)<sub>ss</sub>, and (Ti, V)<sub>ss</sub>, respectively. The solid solution existed in both matrix Ti and matrix V. In the Ti-V binary phase diagram (Fig. 7B), Ti and V can form continuous solid solutions, including BCC (β-Ti,

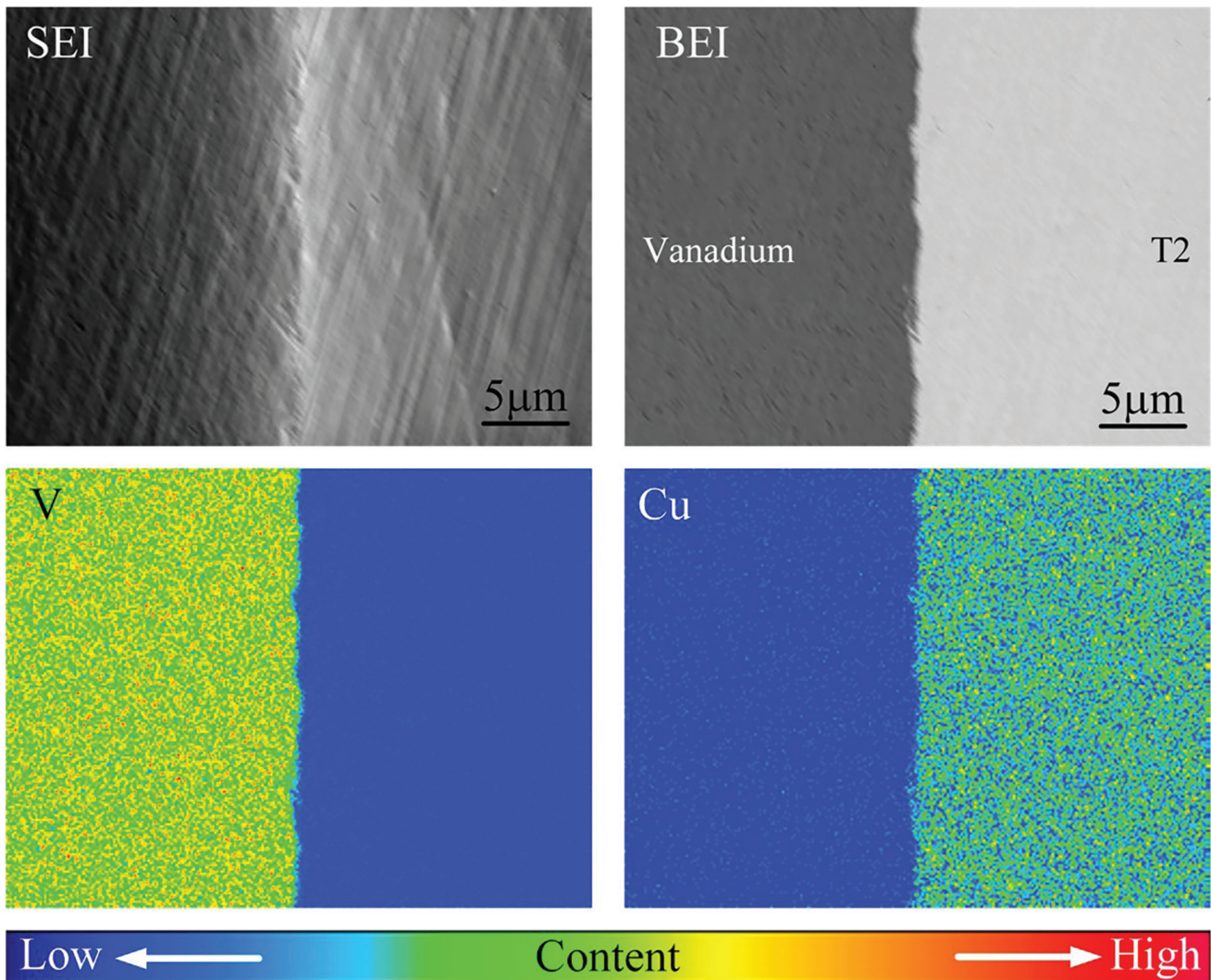


Fig. 5 – Elemental mapping results for the diffusion layer between V and T2 at 860°C for 60 min.

$V)_{ss}$  and BCC ( $\beta$ -Ti, V) $_{ss}$  + HCP ( $\alpha$ -Ti, V) $_{ss}$ . The V element rapidly reduced the transition temperature of  $\alpha$ -Ti to  $\beta$ -Ti, and the region of solid solution became larger with the decrease of temperature. Therefore, different types of solid solutions formed at the TC4/V interface, while no IMCs generated in the V/T2 interface (Figs. 6C, G). The interfacial microstructure was composed of the FCC + BCC phases (Location D). According to the Cu-V binary phase diagram (Fig. 7A), it was characterized by the absence of compounds and a broad liquid and solid immiscible region. Therefore, a mixed layer of FCC + BCC formed at the interface of V/Cu. In addition, based on the data of line scanning on the V/T2 interface, the atomic migration distance of V and Cu was only 1 μm at 840°C for 45 min (Fig. 7D) compared with 2 μm at 880°C for 60 min (Fig. 7H). This phenomenon reflects that the diffusion of V and Cu atoms was little affected by welding temperature and time.

### TEM Analysis of the Reaction Layer on the TC4/V Interface

It is worth noting that the solid-solution phases produced at the TC4/V interface could be seen by the EPMA. Nevertheless, the quantitative analysis was inadequate. Therefore, a TEM test was employed to further analyze the diffusion behavior of interfacial elements between the TC4 and V interlayer. The positions of the FIB sample for TEM characterization were marked in the diffusion zone of TC4/V. The elemental map scanning results in the reaction layer were detected by the EDS in the TEM – Fig. 8. According to the mapping results, particularly the dispersion of V, the diffusion interface between  $(Ti_6, V)_{ss}$  and  $(Ti_3, V)_{ss}$ , among the TEM specimen, was able to prove. From the dark-field image (DFI), it can be seen that the bright-white phase is  $(Ti_6, V)_{ss}$ , and the dark grey phase is  $(Ti_3, V)_{ss}$ . It should be emphasized that the  $Ti_xV_y$  phases were confirmed by the TEM analysis combined with an XRD phase card.

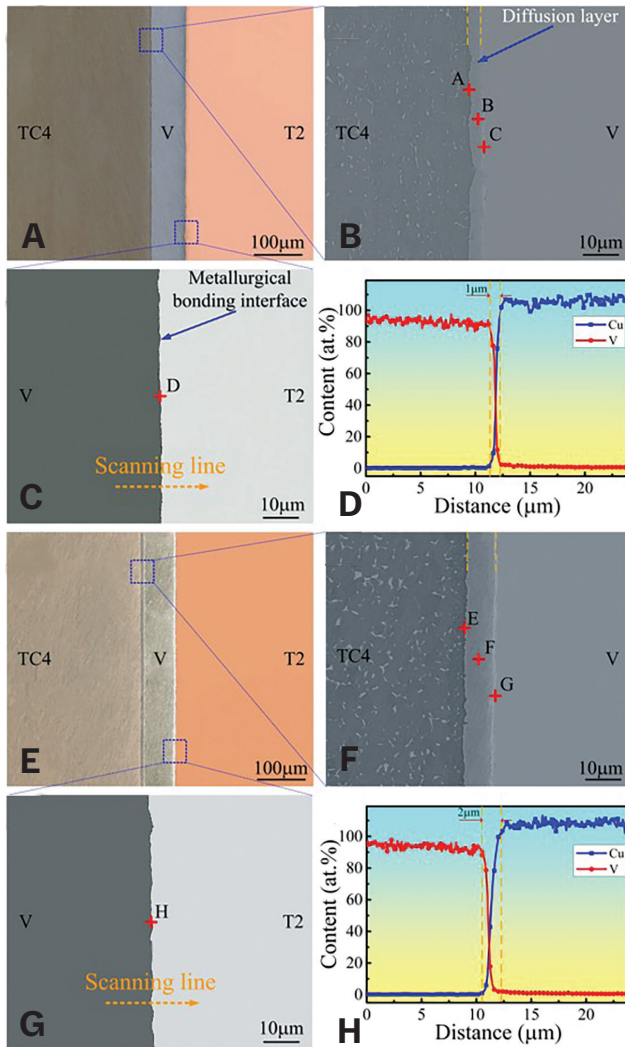


Fig. 6 – Microstructure of the welded joint under different parameters: A – 840°C/45 min; B – TC4/V side; C – V/T2 side; D – result of line scanning on V/T2 side; E – 880°C/60 min; F – TC4/V side; G – V/T2 side; H – result of line scanning on V/T2 side.

To further analyze the crystal structure of different phases of solid solution appearing in the TC4/V interface, TEM images and the patterns of selected area electron diffraction (SAED) for the reaction layer between the TC4 and V interlayer are displayed in Fig. 9. Figures 9A–C show the bright-field image of the  $(Ti_{6'}V)_{ss}$ ,  $(Ti_{3'}V)_{ss}$ , and  $(Ti,V)_{ss}$  reaction layers, respectively. The SAED patterns of positions 1, 2, and 3 presented in Fig. 9 correspond to the phases of  $(Ti_{6'}V)_{ss}$ ,  $(Ti_{3'}V)_{ss}$ , and  $(Ti,V)_{ss}$ , respectively. The pattern of SAED was analyzed down the zone axis of [020] for  $(Ti_{6'}V)_{ss}$ , and three homologous Miller indices – covering (101), (002), and  $(\bar{1}01)$  – were able to be calculated. In addition, the zone axes of  $(Ti_{3'}V)_{ss}$  are [112] and  $[2\bar{1}\bar{4}]$ , corresponding to three Miller indices, including (110), (201), (111) and (201), (121),  $(\bar{1}20)$ , respectively.

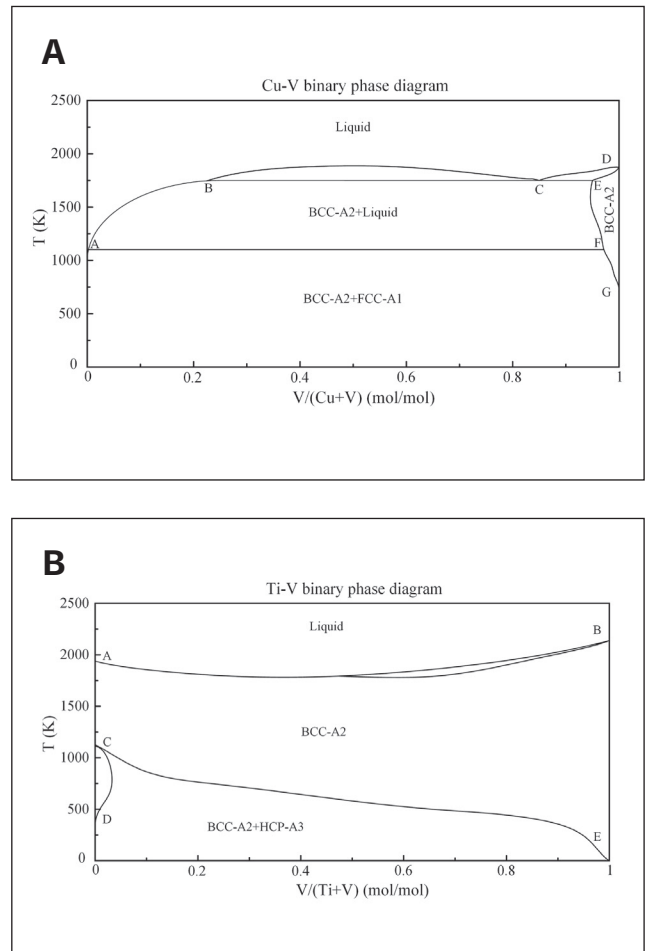


Fig. 7 – Binary phase diagrams: A – Cu-V; B – Ti-V.

The TEM bright-field graphic of the  $(Ti_{6'}V)_{ss}/(Ti_{3'}V)_{ss}$  interface is shown in Fig. 10A. The high-resolution TEM (HRTEM) graphic and patterns of fast Fourier transformation (FFT) between  $(Ti_{6'}V)_{ss}$  and  $(Ti_{3'}V)_{ss}$  are displayed in Figs. 10B and C. Based on the FFT patterns, HRTEM images of  $(Ti_{6'}V)_{ss}$  and  $(Ti_{3'}V)_{ss}$  could be acquired along the corresponding [020] and [112] zone axes. The crystallographic structures between the  $(Ti_{6'}V)_{ss}$  and  $(Ti_{3'}V)_{ss}$  phases in the HRTEM image were (002) and (201), respectively. In addition, the (002) and (201) interplanar spacing was  $d_{(002)} = 0.311$  nm and  $d_{(201)} = 0.276$  nm. The interplanar spacing of  $(Ti_{6'}V)_{ss}$  and  $(Ti_{3'}V)_{ss}$  was very close, so the interfacial energy between the  $(Ti_{6'}V)_{ss}$  and  $(Ti_{3'}V)_{ss}$  was relatively low. This phenomenon illustrated that  $(Ti_{6'}V)_{ss}$  and  $(Ti_{3'}V)_{ss}$  phases were demanded with lower lattice

**Table 5 – Component Analysis Results (at.-%) of Marked Points in Fig. 16**

| Location | Ti   | Cu    | Al   | V     | Possible Phases |
|----------|------|-------|------|-------|-----------------|
| 1        | 0.44 | 88.60 | 0.14 | 10.83 | FCC-Cu + BCC-V  |
| 2        | 1.30 | 0.44  | 0.76 | 97.5  | BCC-V           |
| 3        | 0.75 | 98.65 | 0.13 | 0.47  | FCC-Cu          |
| 4        | 1.16 | 15.96 | 0.05 | 82.83 | BCC-V + FCC-Cu  |
| 5        | 0.39 | 86.63 | 0.18 | 12.80 | FCC-Cu + BCC-V  |
| 6        | 0.17 | 97.84 | 1.05 | 0.94  | FCC-Cu          |
| 7        | 1.02 | 60.59 | 0.19 | 38.21 | FCC-Cu + BCC-V  |
| 8        | 0.88 | 97.17 | 1.12 | 0.83  | FCC-Cu          |

mismatch, which could obtain high joint strength (Ref. 31). The lattice mismatch of the  $(Ti_6, V)_{ss}/(Ti_3, V)_{ss}$  welded interface was able to be obtained using the following function (Ref. 32):

$$F = 2(d_{(002)} - d_{(201)}) / (d_{(002)} + d_{(201)}) \quad (2)$$

where  $d_{(002)} = 0.311$  nm and  $d_{(201)} = 0.276$  nm are d-spacings for  $(Ti_6, V)_{ss}$  and  $(Ti_3, V)_{ss}$ , respectively, as displayed in Figs. 10B and C. Therefore, the lattice mismatch of  $(Ti_6, V)_{ss}$  and  $(Ti_3, V)_{ss}$  was obtained to be 11.9%, which demonstrated that the  $(Ti_6, V)_{ss}/(Ti_3, V)_{ss}$  interface was approximately coherent with low strain energy. Meanwhile, a large number of dislocations may form at the  $(Ti_6, V)_{ss}/(Ti_3, V)_{ss}$  interface, reducing the strain energy.

## Diffusion Behavior and Kinetics

Based on the information of line scanning for Ti, V, and Al, the width of the diffusion zone was able to be acquired. The consequences of line scanning along the interface of TC4/V under different parameters were obtained – Fig. 11.

Ti and V distributed in the diffusion layer, but Al rarely distributed in the reaction layer. Furthermore, the width of the

diffusion zone increased with increasing welding temperature and holding time. The minimum and maximum widths of the reaction zone near the TC4 side were 3.2 and 10  $\mu$ m at 840°C for 45 min and 880°C for 60 min, respectively. Based on the data of line scanning, the reaction zone near the TC4 side was mainly a solid solution with matrix titanium, while the bright-white band near the V side was a solid solution with matrix vanadium due to the different diffusion coefficients between titanium and vanadium (Ref. 33).

To illustrate the influence of welding temperature on atomic movement behaviors of reaction zones, we discussed the fitted growth curve and obtained the reaction activation energy. The average thickness and constant coefficients for the diffusion layer of TC4/V with various parameters are listed in Table 4.

The data indicated that with the welding temperature and time enlarged, the average thickness of the diffusion zone also enlarged. The relation of the width for reaction zones to welding time was able to be obtained with the following function (Ref. 34):

$$w^2 = Dt \quad (3)$$

where  $w$  is the width of the diffusion zone (m),  $D$  is the coefficient of atomic migration ( $m^2/s$ ), and  $t$  is the holding time (s).

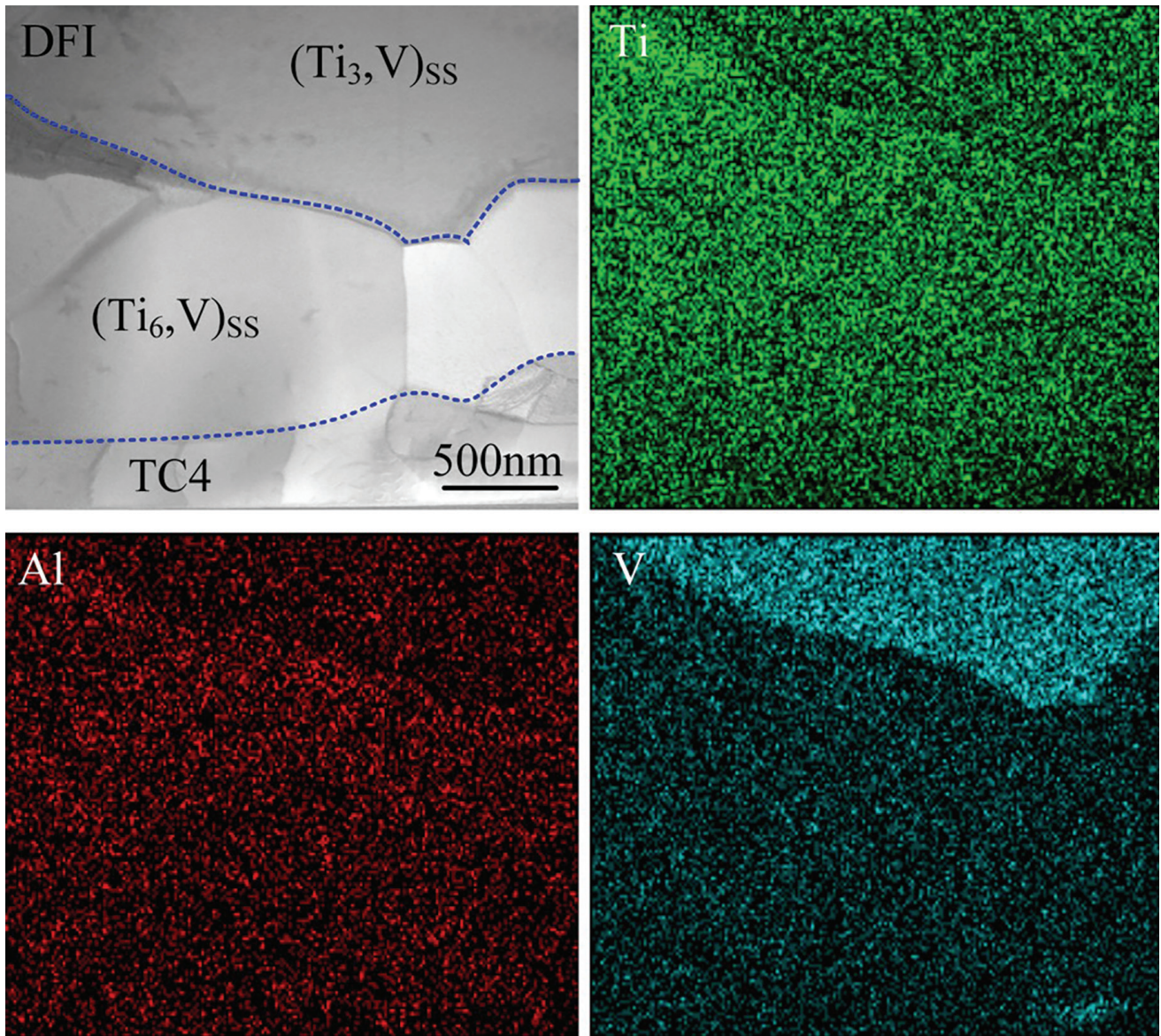


Fig. 8 – Elemental mapping results in the reaction zone of the TC4/V interface analyzed by the TEM equipped with the EDS.

The relation of welded temperature and growth activation energy complied with the formula of Arrhenius (Ref. 35):

$$D = D_0 \exp(-Q/RT) \quad (4)$$

where  $D_0$  is the growth constant coefficient ( $\text{m}^2/\text{s}$ ),  $Q$  is the growth activation energy ( $\text{kJ}/\text{mol}$ ),  $R$  is the gas constant ( $8.314 \text{ J}/\text{K} \cdot \text{mol}$ ), and  $T$  is the welding temperature (K). A new relation about function between the thickness of the reaction zone and the welding temperature was able to be described with the following by combining Equations 3 and 4:

$$\text{Ln}w = \left(\frac{Q}{2R}\right)\left(-\frac{1}{T}\right) + \frac{1}{2}\text{Ln}(tD_0) \quad (5)$$

In the study, the reaction time was constant, while the welding temperature was variable. The relationship between the width of the same reaction zone and activation energy at different welding temperatures can be calculated and fitted. The fitting consequence of the growth behavior for the reaction layer between TC4 and V is listed in Fig. 12.

The width of the reaction zone grew in a parabolic relationship with an equation of welding temperature (Fig. 12A). It was calculated that the growth activation energy of the diffusion layer for the TC4/V interface was  $226.6 \text{ kJ}/\text{mol}$  at different temperatures for 60 min (Fig. 12B). Therefore, the diffusion activation energy to form a stable solid solution between titanium and vanadium was  $226.6 \text{ kJ}/\text{mol}$ . It is worth noting that the growth activation energy for products forming between titanium and vanadium has not been previously reported in literature. The atomic migration was

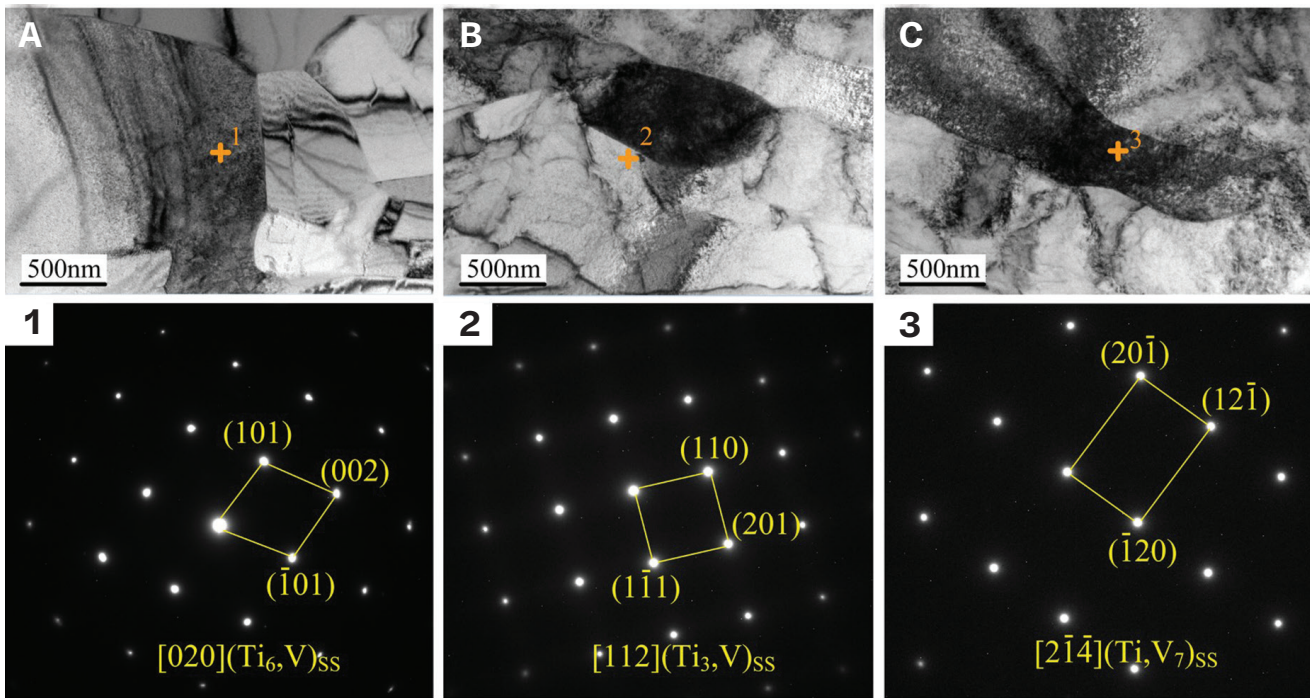


Fig. 9 – TEM graphics of the diffusion layer of the TC4/V interface at 860°C for 60 min; bright-field graphic of: A –  $(Ti_6, V)_{ss}$  reaction layer; B –  $(Ti_3, V)_{ss}$  reaction layer; and C –  $(Ti, V_7)_{ss}$  reaction layer. 1–3 – The SAED patterns of marked positions.

Table 6 – EDS Component Analysis Results (at.-%) of Marked Points in Fig. 17

| Location | Ti   | Cu    | Al   | V     | Possible Phases |
|----------|------|-------|------|-------|-----------------|
| 1        | 0.29 | 0.85  | 0.20 | 98.66 | BCC-V           |
| 2        | 0.16 | 63.59 | 1.05 | 35.20 | FCC-Cu + BCC-V  |
| 3        | 1.44 | 0.50  | 0.56 | 97.50 | BCC-V           |
| 4        | 0.15 | 98.17 | 0.05 | 0.83  | FCC-Cu          |

achieved through the generation of thermal defects. Thus, reaction activation energy could be obtained to generate these thermal defects.

## Joint Strength

The shear test was applied to explore the influence of V foil on the shear performance of the welded joints with dif-

ferent parameters. To measure the shear performance of the welded joints, a self-designed fixture for the shear experiment was prepared, as displayed in Fig. 1C. The welded joints were put in this equipment, and the position of the welded interface was upright. The shear force was inflicted on TC4 base material with an axial force until the welded joint failed. Welding temperature and time affected the atomic diffusion, interface reaction, and microstructure of the joint. The medial

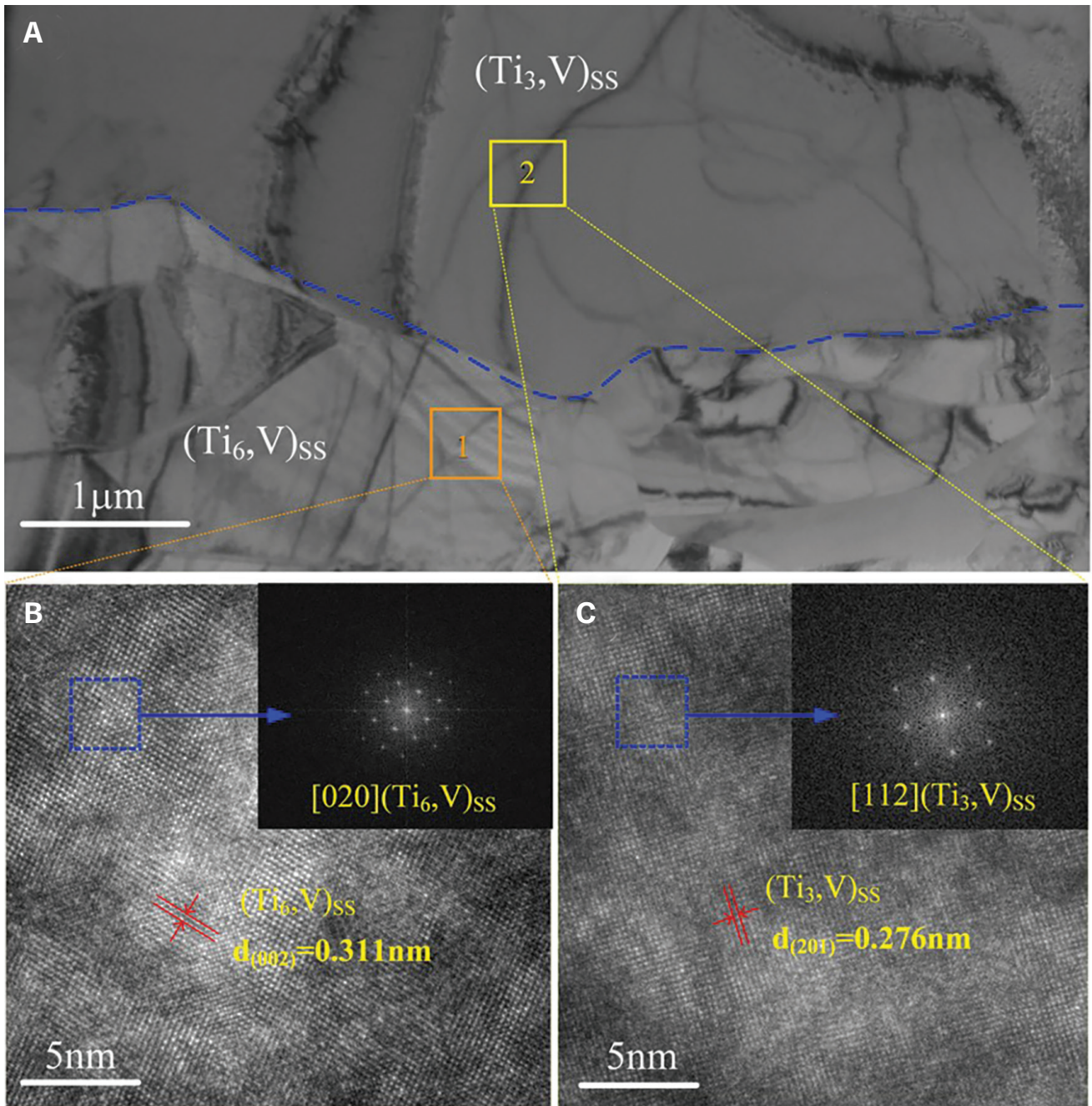


Fig. 10 – A – TEM bright-field graphic of the  $(Ti_6, V)_{ss} / (Ti_3, V)_{ss}$  interface; B – HRTEM graphic and FFT patterns of  $(Ti_6, V)_{ss}$ ; C – HRTEM graphic and FFT patterns of  $(Ti_3, V)_{ss}$ .

shear performance of welded joints under various process parameters is displayed in Fig. 13.

The shear performance increased gradually with the increase of welding temperature and time (Fig. 13A). It is important to emphasize that the shear performance of the joint enlarged first but then descended with the increase of welding temperature for 60 min. The highest shear performance of the joint reached 160 MPa obtained at 860°C for 60 min, while the minimum shear performance of the welded joint was only 90 MPa under 840°C/30 min due to

the interfacial defect. With the welding temperature and time increase, the atoms of elements diffused fully in the interface, resulting in high-joint shear performance. However, the shear performance of the welded joint obtained under 880°C/60 min decreased slightly compared with that of the joint at 860°C for 60 min, which was caused by a thick diffusion layer and coarse grain (Ref. 36). Figure 13B compares the work of other scholars on the performance of the welded joint of titanium to copper, including no interlayer, single interlayer, and multi-interlayers. Su et al. (Ref. 37) studied vacuum diffusion welding of TC4/OFC, and the shear strength of joints

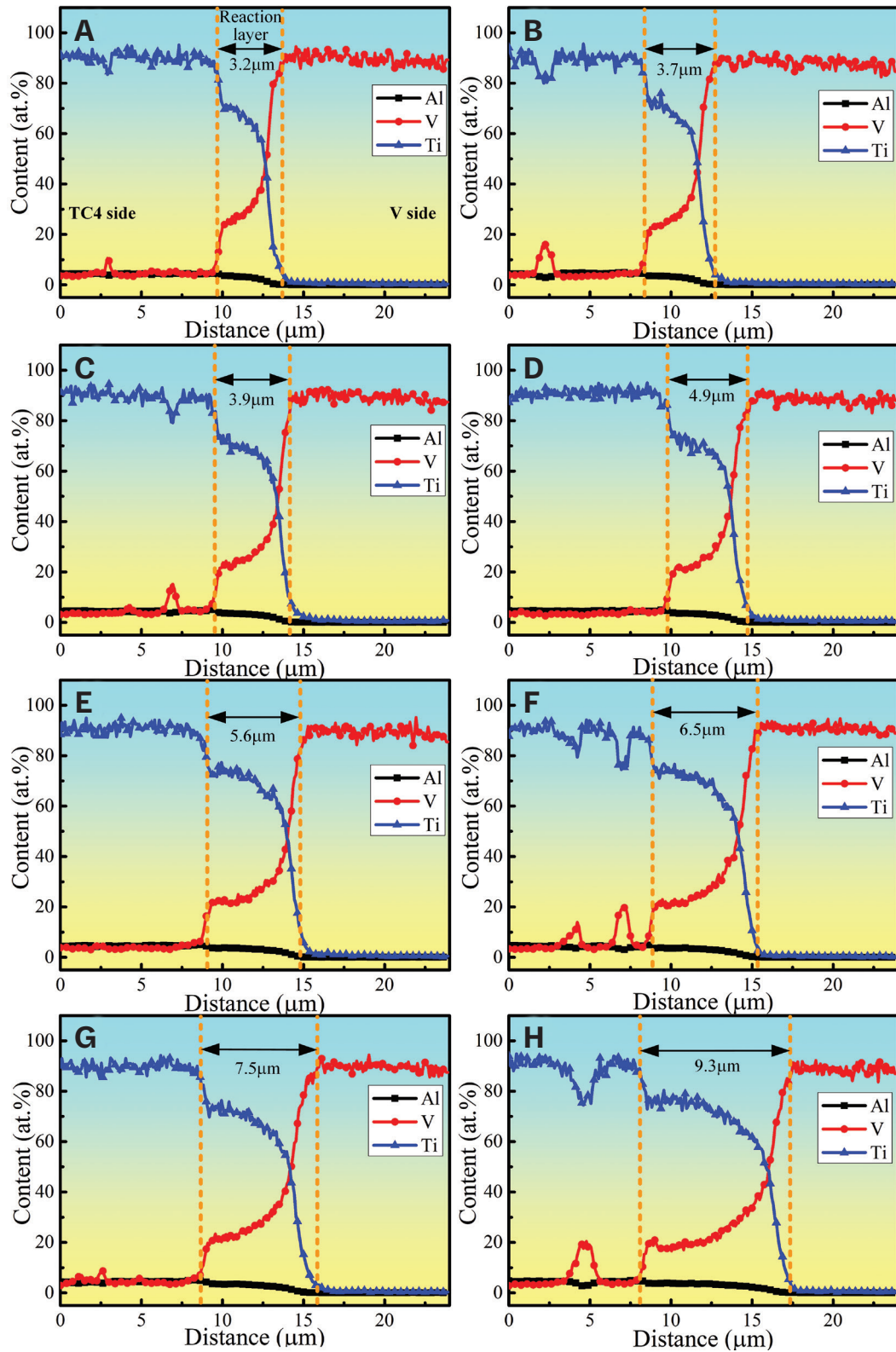


Fig. 11 – Consequences of line scanning along the diffusion zone of the TC4/V interface under various parameters: A – 840°C/45 min; B – 840°C/60 min; C – 860°C/30 min; D – 860°C/45 min; E – 860°C/60 min; F – 880°C/30 min; G – 880°C/45 min; H – 880°C/60 min.

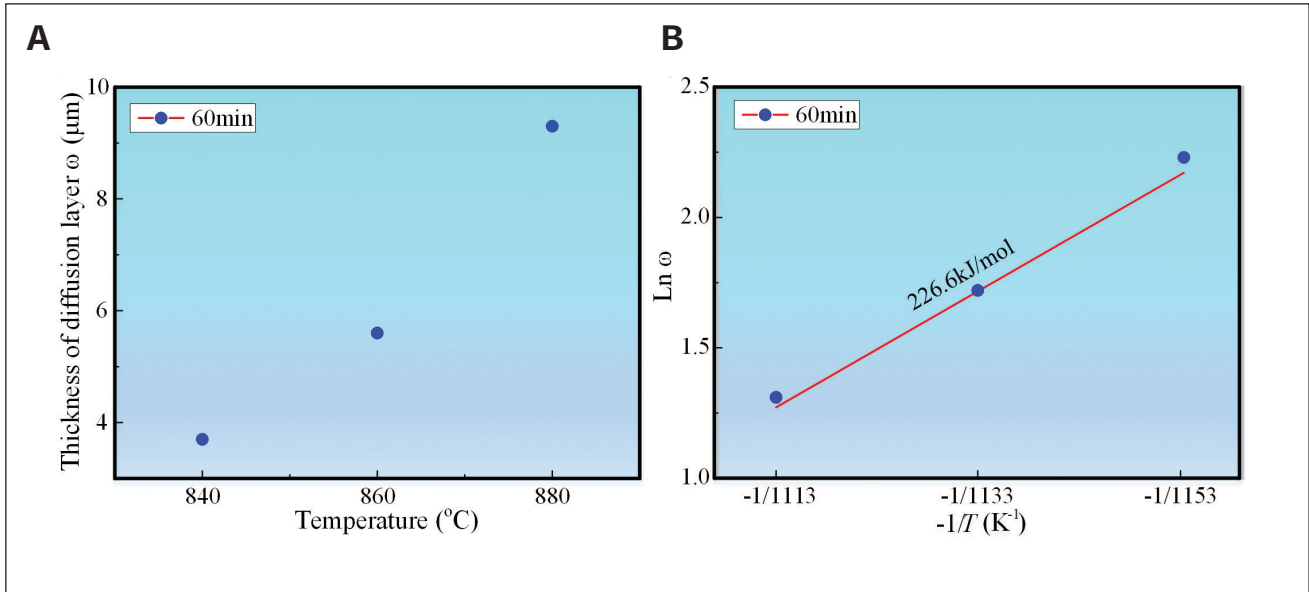


Fig. 12 – Thickness and reaction activation energy for the reaction layer of TC4/V under different temperatures: A – Thickness of diffusion layer; B – growth activation energy.

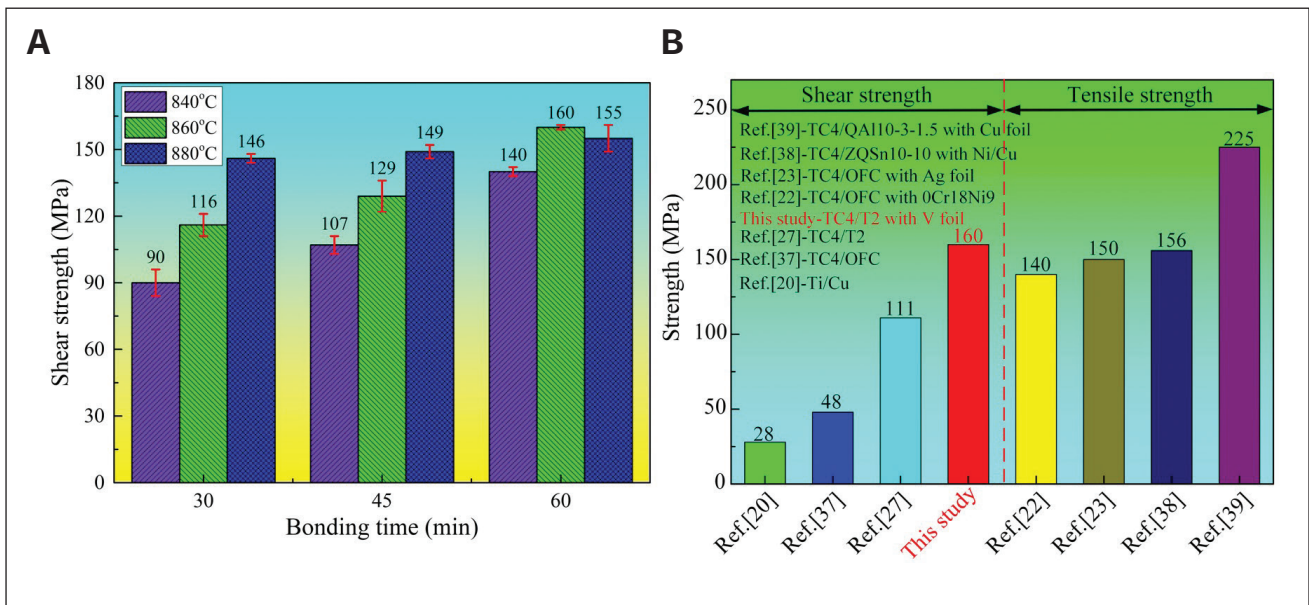


Fig. 13 – Bonded joint strength: A – Medial shear performance of welded joints under various parameters; B – joint strength between this research and other research.

reached 48 MPa. Zhao et al. (Ref. 38) revealed the effect of transitional interlayers on the performances of diffusion welded joints of TC4 titanium alloy to ZQSn10-10 alloy. The maximum tensile performance of the welded joint was only 156 MPa with Ni/Cu interlayers. It is worth mentioning that the shear performance of the TC4/T2 welded joint without an interlayer in our previous study reached 111 MPa (Ref. 27). All the shear performance of the welded joint in other studies was much lower than that in the test. The tensile performance of the joints obtained between the Ti-6Al-4V

and QAl10-3-1.5 alloys at 850°C for 60 min under 10 MPa (Ref. 39) was higher than that in this study. In addition, the tensile strength of the joint obtained between TC4 and OFC with the OCr18Ni9 and Ag interlayer was 140 and 150 MPa, respectively (Refs. 22, 23). Therefore, the tensile strength of the joint in Refs. 22, 23, and 38 demonstrated the advantage of a V interlayer on diffusion welding of TC4/T2. This result also revealed that the solid solution appeared in the TC4/V interface, and metallurgical bonding between V and Cu were superior to the IMCs formed between titanium and copper,

**Table 7 – Constant Factor and Growth Activation Energy of Ti, V, and Cu (Ref. 34)**

| Elements | Constant Factor ( $D_0$ )/m <sup>2</sup> /s | Growth Activation Energy (Q)/kJ/mol |
|----------|---|-------------------------------------|
| Ti       | $1.9 \times 10^{-7}$                        | 152.8                               |
| Cu       | $1.9 \times 10^{-5}$                        | 196.4                               |
| V        | $2.9 \times 10^{-5}$                        | 309.6                               |
| Ti in V  | $1.0 \times 10^{-5}$                        | 285.0                               |
| V in Ti  | $2.1 \times 10^{-5}$                        | 209.0                               |
| Cu in V  | $1.8 \times 10^{-5}$                        | 266.2                               |
| V in Cu  | $2.5 \times 10^{-4}$                        | 215.0                               |

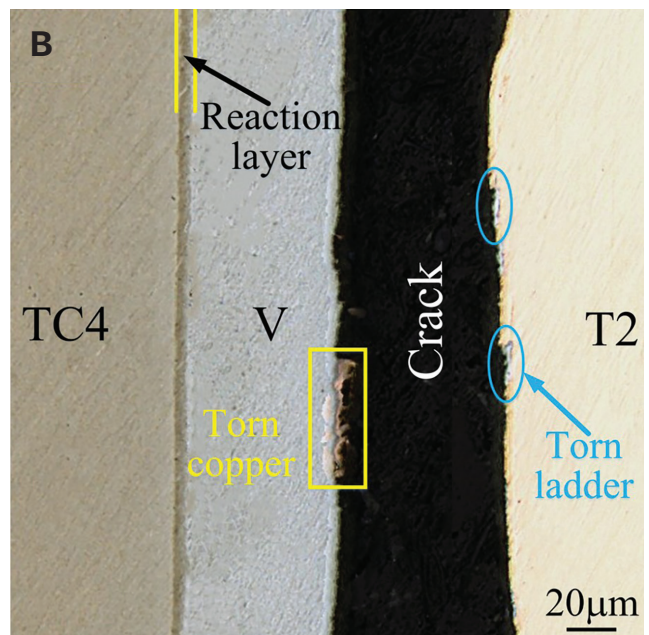
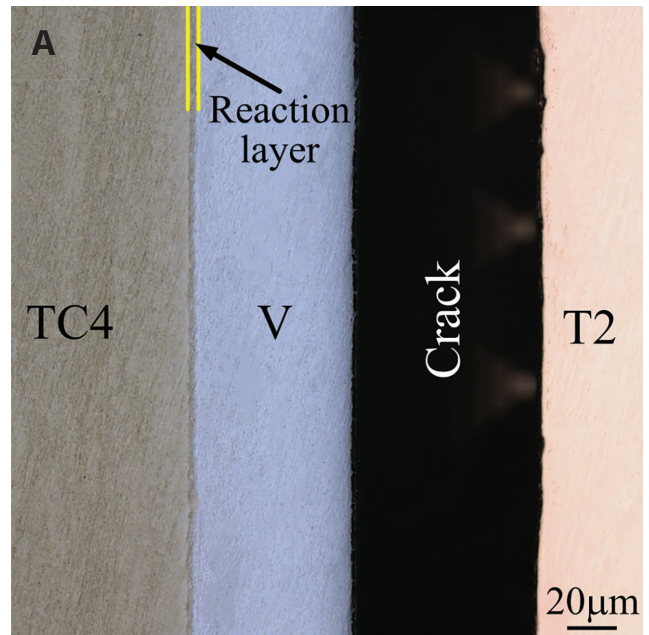


*Fig. 14 – Intersecting surface morphologies of the fracture path for the failed joint under different parameters: A – 840°C/45 min; B – 860°C/60 min.*

which was also one of the reasons for improving the performance of TC4 and T2 diffusion welded joints.

### Fracture Analysis

Figures 14A and B show the intersecting surface morphologies of the fracture path for the joints welded at 840°C for 45 min and 860°C for 60 min, respectively. The welded joint fractured along the interface of V/T2, illustrating that the V/T2 interface was a weaker part compared with that of

TC4/V. Moreover, the fracture interface of the welded joints obtained under 840°C/45 min was smooth and flat (Fig. 14A). The joints obtained at 860°C for 60 min also fractured along the interface of V/T2, but partially torn copper bound to the V side and some torn ladders appeared on the T2 side (Fig. 14B). These torn ladders could absorb more shear energy (Ref. 2), which caused the shear strength of the joints to be higher than that of the joints without secondary cracks.

To confirm the phases on the failed joints, Fig. 15 exhibits the XRD patterns of both sides of the failed joints under

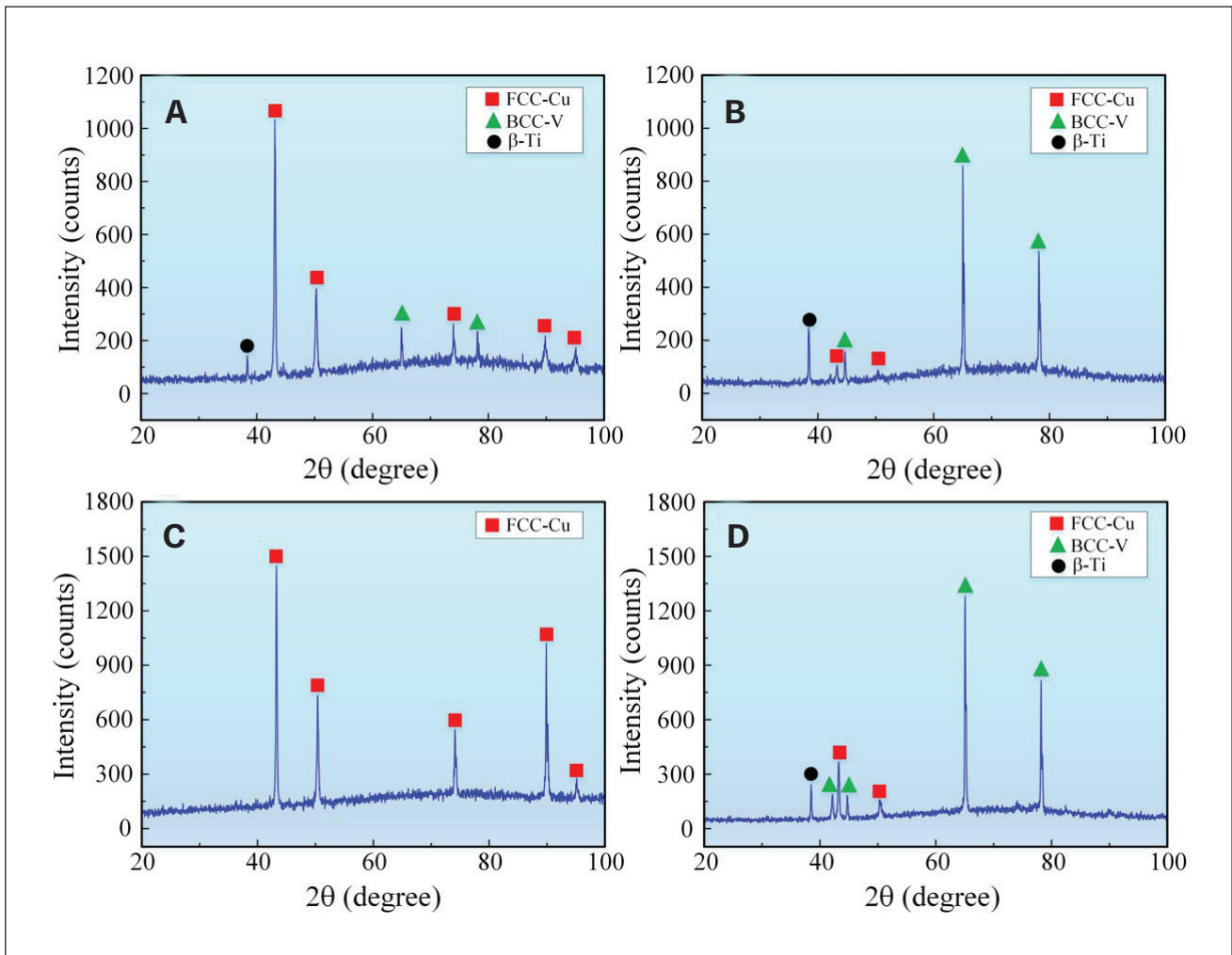


Fig. 15 – Phase composition of the fracture joint at 840°C for 45 min: A – T2 copper side; B – TC4 titanium alloy side. At 860°C for 60 min: C – T2 copper side; D – TC4 titanium alloy side.

840°C for 45 min and 860°C for 60 min, respectively. FCC-Cu, BCC-V, and  $\beta$ -Ti microstructure were detected on both broken sides of the failed joint at 840°C/45 min. However, only the FCC-Cu phase was detected on the T2 side, but FCC-Cu, BCC-V, and  $\beta$ -Ti phases were found on the TC4 side as the welding temperature and time were correspondingly 860°C and 60 min.

The fracture surfaces of the failed joints obtained under different diffusion parameters are displayed in Fig. 16. Figures 16A and B present the morphology of the joints on the TC4 and T2 sides under 840°C/45 min, respectively. In Fig. 16A, the fracture surface has some discontinuous ridge shape, belonging to a typical cleavage fracture mode. On the T2 side, the fracture feature with a river pattern and dimples is found in Fig. 16B, which was characterized by a typical ductile and dissociative fracture. Relatively, the morphology of the joint obtained under 860°C/60 min was various from that obtained under 840°C for 45 min. Some dimples formed on the morphology of the failed joint on the TC4 side (Fig. 16C), indicating a ductile fracture. Nevertheless, the fracture fea-

ture of the failed joint was composed mainly of a river pattern and ladder topography, which was a cleavage fracture mode.

According to Cao et al. (Ref. 40), the cleavage fracture belonged to a sort of brittle transgranular fracture, which can happen in the special crystal planes under a small index. Thus, the welded joint acquired with 860°C/60 min was more ductile than that at 840°C/45 min, which presented the larger shear performance. To explore the formation of phase on the failed joints, the chemical composition of locations marked in Fig. 16 are shown in Table 5. On the TC4 and T2 sides, FCC-Cu + BCC-V (Locations 1, 5, and 7), BCC-V + FCC-Cu (Location 4), BCC-V (Location 2), and FCC-Cu (Locations 3, 6, and 8) were detected, which possessed specific fracture features. The BCC-V + FCC-Cu and BCC-V phases mainly emerged the cleavage feature accompany some cleavage steps and facets. The FCC-Cu + BCC-V phase was characterized mainly by some tiny folds. The FCC-Cu phase displayed many smooth planes.

In addition, our research revealed a new finding for the fracture feature of joints. The special fracture feature of the welded joint at 880°C for 60 min is shown in Fig. 17. On the

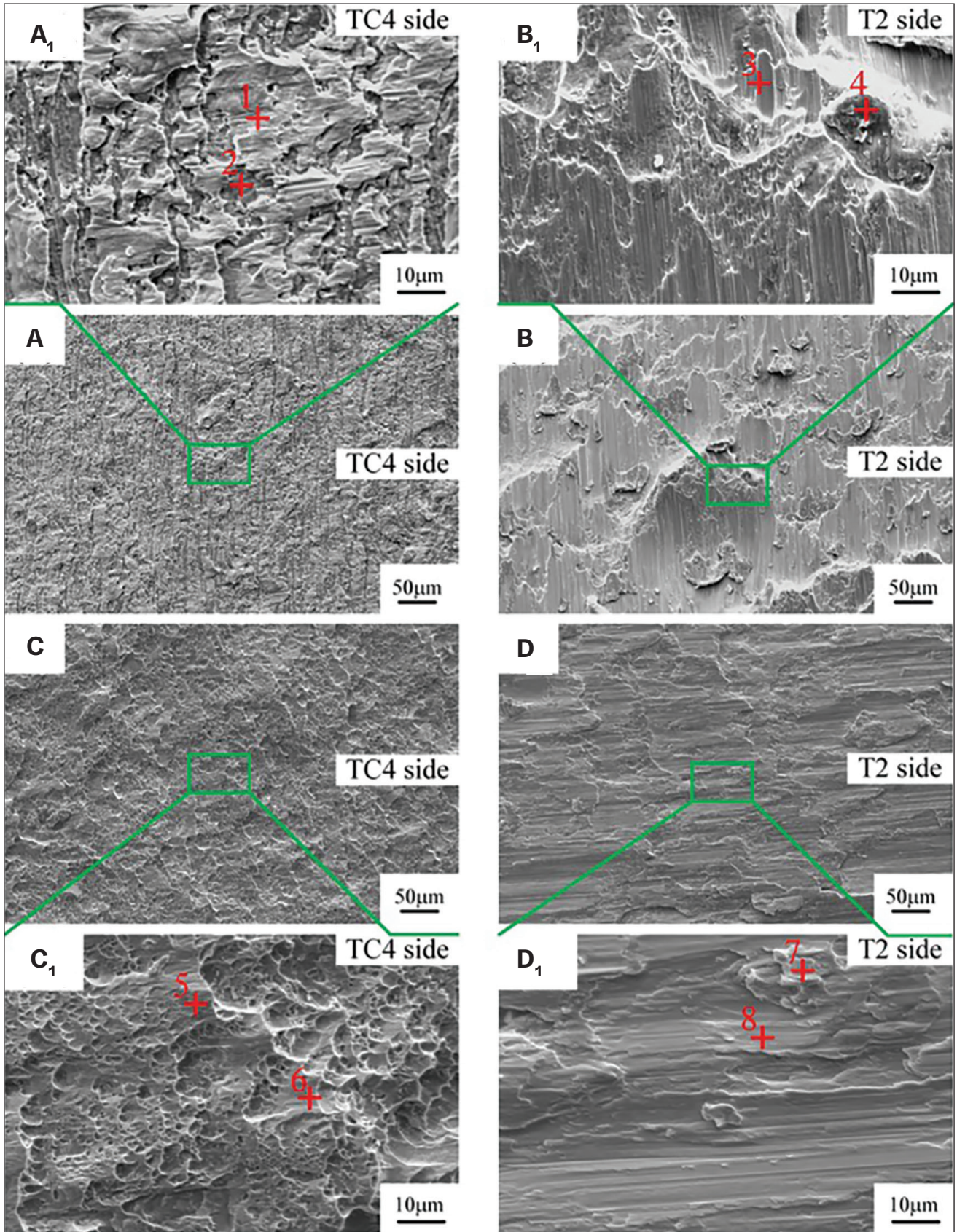


Fig. 16 – Fracture morphologies of the failed joints at 840°C for 45 min: A – TC4 titanium alloy side; B – T2 copper side. At 860°C for 60 min: C – TC4 titanium alloy side; D – T2 copper side.

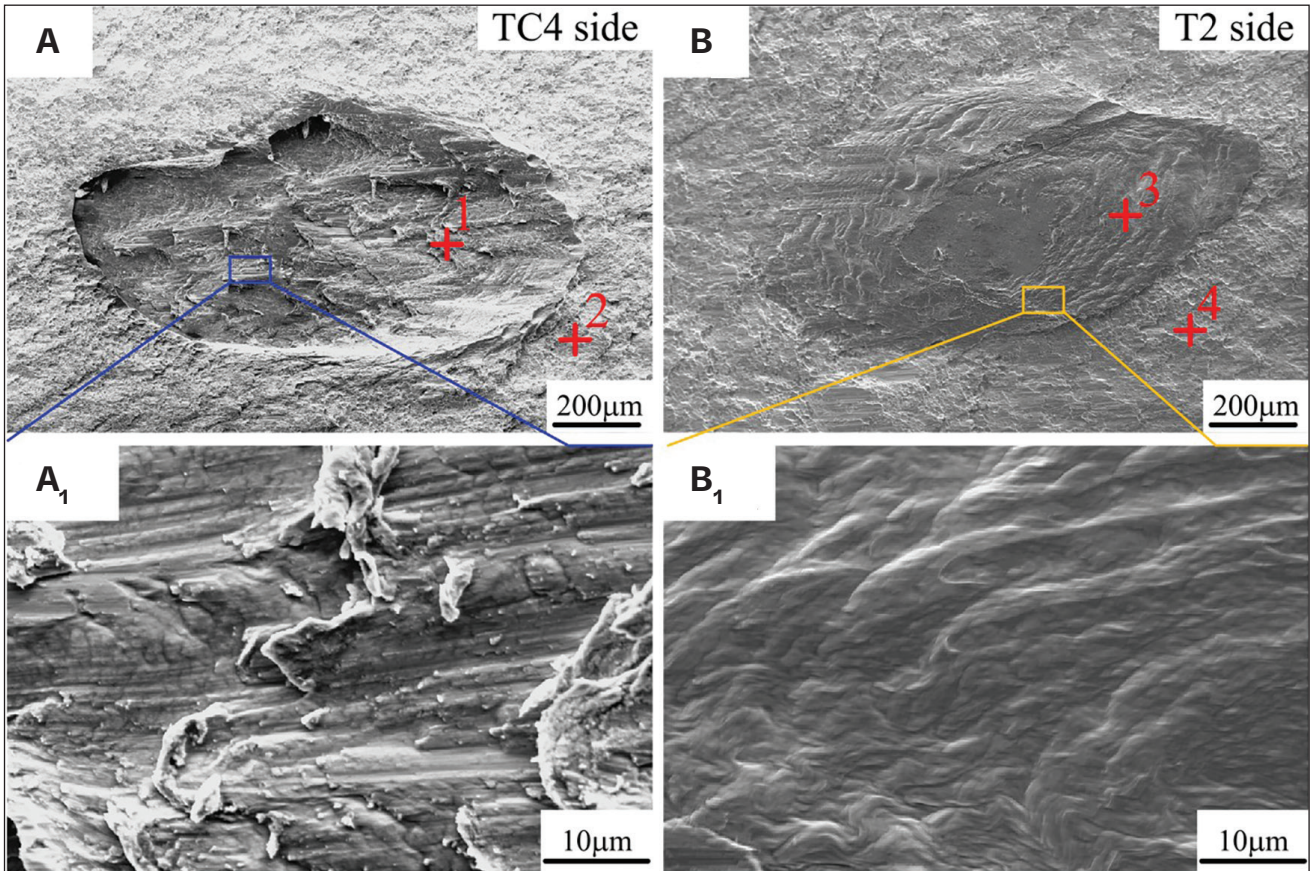


Fig. 17 – Special fracture morphology of the welded joint at 880°C for 60 min: A – TC4 titanium alloy side; B – T2 copper side; A<sub>1</sub> and B<sub>1</sub> – corresponding high magnification views.

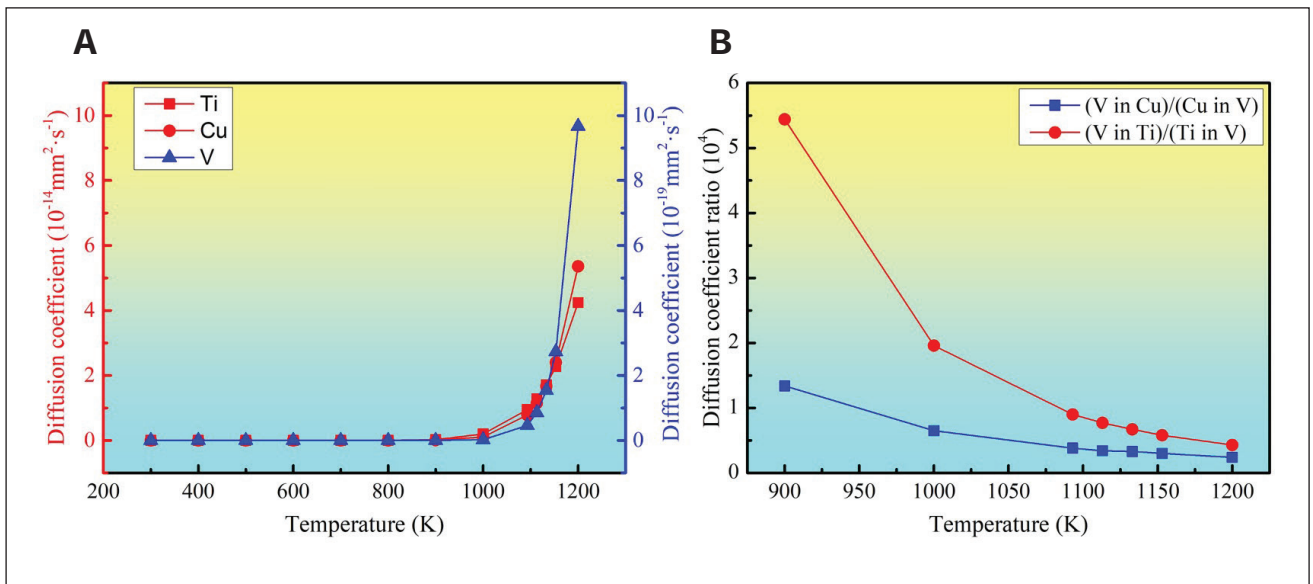


Fig. 18 – Function of elements diffusion coefficient to welding temperature: A – Auto-diffusion of Ti, V, and Cu; B – interdiffusion coefficient ratio of Ti-V and V-Cu.

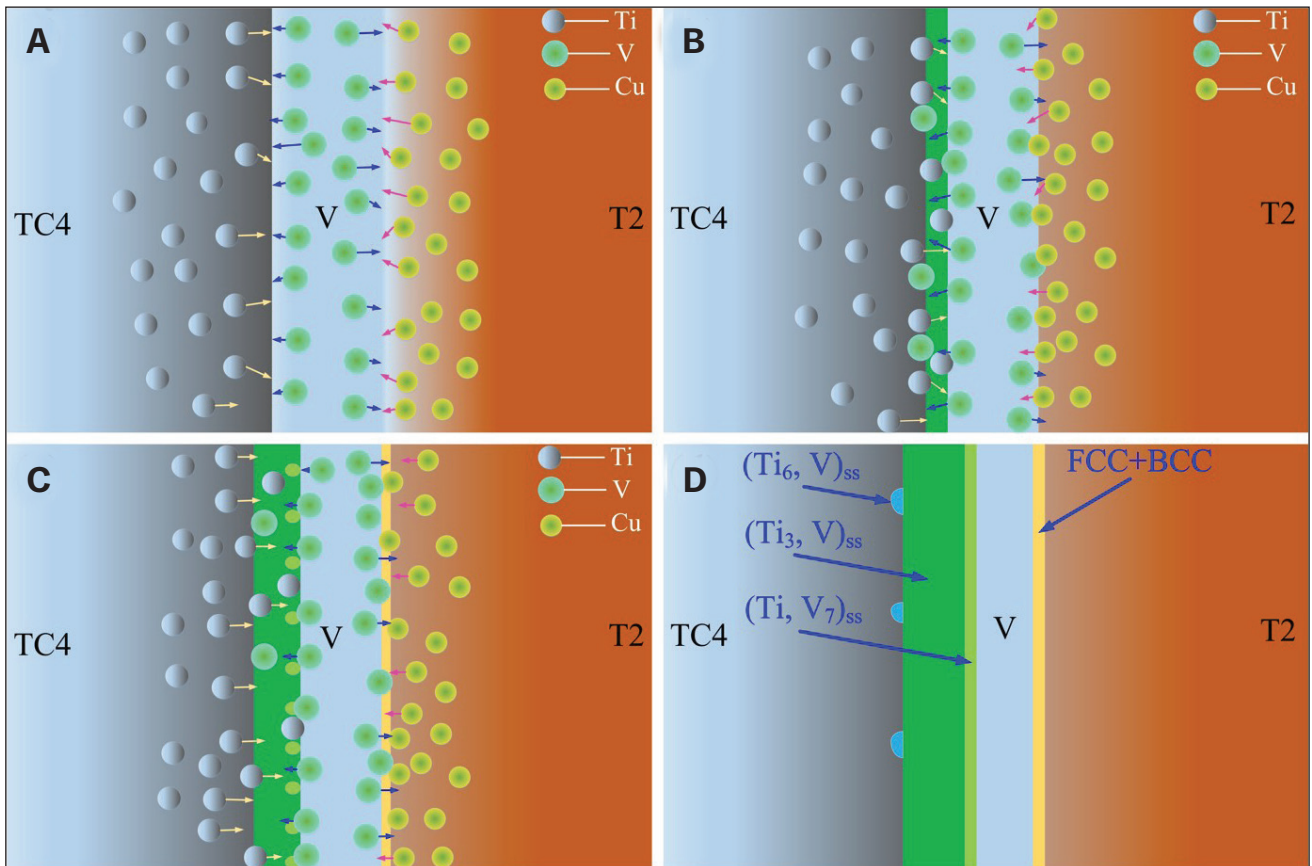


Fig. 19 – Process of microstructure evolution for the diffusion welded joint between titanium alloy and copper with V foil as the interlayer: A – Initial touch; B – motion of atoms; C – atomic diffusion reaction; D – formation of reaction product.

TC4 side, a basin fault zone appeared on the fracture surface, which was characterized mainly by rough cleavage steps and facets (Fig. 17A1), while a raised hill fault zone was displayed on the T2 side, which was a cleavage feature with a smooth river pattern and ladder topography. The EDS chemical composition of the locations are listed in Table 6. The basin and hill fault zones fractured along the vanadium layer based on the BCC-V phase detected at locations 1 and 3. This special fracture mode could absorb some energy when the specimen was sheared. Therefore, the shear strength of the welded joints could be further improved.

## Diffusion Mechanism

The driving force of diffusion welding for Ti/V and V/Cu hinges on the coefficient of diffusion; concentration gradient; and crystal structure for Ti, V, and Cu. Among them, the diffusion coefficient is decided through the reaction activation energy and welding temperature, which is a dynamic value that changes during the diffusion process (Ref. 41). Table 7 displays the diffusion factor and reaction activation energy of Cu, V, and Ti.

Based on Equation 4, the auto-diffusion coefficient of Ti, V, and Cu and the function between the diffusion coefficient

and welding temperature for interdiffusion of Ti, V, and Cu can be acquired. The relationship between diffusion coefficient and welding temperature is listed in Fig. 18. The self-diffusion coefficient of Ti, V, and Cu increased with the augmentation of welding temperature emerged as a form of exponent, and the diffusion coefficient of Ti, V, and Cu became sufficient (Fig. 18A). The auto-diffusion coefficient of Ti was close to that of Cu at the identical welding temperature, while the auto-diffusion coefficient of vanadium was several orders of magnitude smaller than that of titanium and copper. Therefore, the diffusion velocity of titanium and copper was more rapid than that of V at the same temperature. In Fig. 18B, the diffusion coefficient of V in Ti is much larger than that of Ti in V, which has a difference of several orders of magnitude. The interdiffusion coefficient ratio of V in Ti and Ti in V decreased with the augmentation of temperature. Therefore, the effect of welding temperature on the atomic migration of V in the Ti matrix was greater than that of Ti in the V matrix when the temperature was below 1200°K (926.85°C/700.33°F), meaning that the diffusion ability of V into Ti was greater than that of Ti into V. In addition, the diffusion coefficient of V in Cu was faster than Cu in V, illustrating that the diffusion capacity of the V element was stronger than that of the Cu element at the welded interface.

The process of microstructure evolution for a diffusion welded joint between titanium alloy and copper with V foil as the interlayer is exhibited in Fig. 19. When the temperature reached the diffusion temperature, the atoms at the Ti/V and V/Cu interfaces diffused each other. Ti-V solid solution formed at the interface of TC4 and V with continuous diffusion reaction, while the V/T2 interface was a metallurgical bonding with neither IMCs nor solid solutions. With the decrease of diffusion element concentration, different types of solid solutions formed at the TC4/V interface, including solid-solution phases of  $(\text{Ti}_{61}\text{V})_{\text{ss}}$ ,  $(\text{Ti}_{31}\text{V})_{\text{ss}}$ , and  $(\text{Ti}, \text{V}_{7})_{\text{ss}}$ . However, only FCC-Cu + BCC-V phases formed at the interface of V/T2 due to metallurgical bonding between V and Cu. The solid-solution structure between Ti and V was stronger than the metallurgical bonding between V and Cu according to the fracture morphology of the joint. Therefore, the solid-solution structure formed between dissimilar materials was able to obviously enhance the performance of the welded joint.

## Conclusions

Vacuum diffusion welding of TC4/T2 with pure V foil as an interlayer under different parameters was discussed. The microstructure evolution, shear properties, and element diffusion behavior of the welded joint were revealed. The main results are drawn as follows:

1) Vanadium foil effectively prevented the direct diffusion reaction of titanium and copper from producing IMCs. The solid-solution phases of  $(\text{Ti}_{61}\text{V})_{\text{ss}}$ ,  $(\text{Ti}_{31}\text{V})_{\text{ss}}$ , and  $(\text{Ti}, \text{V}_{7})_{\text{ss}}$  formed in the interface of TC4/V. The crystallographic orientations of  $(\text{Ti}_{61}\text{V})_{\text{ss}}$ ,  $(\text{Ti}_{31}\text{V})_{\text{ss}}$ , and  $(\text{Ti}, \text{V}_{7})_{\text{ss}}$  phases in the HRTEM image were (002), (201), and (121), respectively. The lattice mismatch between  $(\text{Ti}_{61}\text{V})_{\text{ss}}$  and  $(\text{Ti}_{31}\text{V})_{\text{ss}}$  was calculated to be 11.9% with low strain energy.

2) The highest shear strength of the welded joint reached 160 MPa, made at 860°C for 60 min, while the minimum shear strength of the welded joint was only 90 MPa under 840°C/30 min due to insufficient diffusion and interfacial defects. The crack propagation path of all joints occurred along with the interface of V/T2. The fracture characteristics of the failed joints were mainly composed of the river pattern and ladder topography, which was a cleavage fracture mode. FCC-Cu, BCC-V, and  $\beta$ -Ti microstructure were detected on both broken sides of the failed joint. The interface of V/T2 formed a metallurgical bonding with neither IMCs nor solid solutions.

3) The reaction activation energy of the reaction product generated at the TC4/V interface was 226.6 kJ/mol at different welding temperatures for 60 min. The diffusion rate of titanium and copper was faster than that of vanadium at the same temperature, and the influence of welding temperature on the atomic diffusion of vanadium in titanium was greater than that of titanium in vanadium. The solid-solution structure formed between Ti and V was stronger than the metallurgical bonding between V and Cu.

## Acknowledgments

This work was supported by the National Natural Science Foundation of China (52275314 and 52075074) and the Collaborative Innovation Center of Major Machine Manufacturing in Liaoning.

## References

1. Ziegelheim, J., Hiraki, S., and Ohsawa, H. 2007. Diffusion bondability of similar/dissimilar light metal sheets. *Journal of Materials Processing Technology* 186(1–3): 87–93. DOI: 10.1016/j.jmatprotec.2006.12.020
2. Cheng, Z., Huang, J., Ye, Z., Yang, J., and Chen, S. 2019. Butt brazing of titanium alloys/stainless steel plates by MIG-TIG double-sided arc welding process with copper filler metal. *Journal of Materials Research and Technology* 8(1): 1566–1570. DOI: 10.1016/j.jmrt.2018.06.009
3. Peng, Y., Li, J., Shi, J., Li, S., and Xiong, J. T. 2021. Microstructure and mechanical properties of diffusion bonded joints of high-entropy alloy  $\text{Al}_5(\text{HfNbTiZr})_{95}$  and TC4 titanium alloy. *Journal of Materials Research and Technology* 11: 1741–1752. DOI: 10.1016/j.jmrt.2021.02.003
4. Zhu, F., Peng, H., Li, X., and Chen, J. 2018. Dissimilar diffusion bonding behavior of hydrogenated  $\text{Ti}_2\text{AlNb}$ -based and Ti-6Al-4V alloys. *Materials & Design* 159: 68–78. DOI: 10.1016/j.matdes.2018.08.034
5. Mo, D., Song, T., Fang, Y., Jiang, X., Luo, C., Simpson, M., and Luo, Z. 2018. A review on diffusion bonding between titanium alloys and stainless steels. *Advances in Materials Science and Engineering* 16: 1–15. DOI: 10.1155/2018/8701890
6. Chen, S., Soh, A., and Ke, F. 2005. Molecular dynamics modeling of diffusion bonding. *Scripta Materialia* 52(11): 1135–1140. DOI: 10.1016/j.scriptamat.2005.02.004
7. Cao, C., Letzig, T., Görler, G., and Herlach, D. 2001. Liquid phase separation in undercooled Co-Cu alloys processed by electromagnetic levitation and differential thermal analysis. *Journal of Alloys and Compounds* 325(1–2): 113–117. DOI: 10.1016/S0925-8388(01)01276-2
8. Li, S., Li, J., Shi, J., Peng, Y., Peng, X., Sun, X., Jin, F., Xiong, J., and Zhang, F. 2022. Microstructure and mechanical properties of transient liquid phase bonding DD5 single-crystal superalloy to CrCoNi-based medium-entropy alloy. *Journal of Materials Science & Technology* 96: 140–150. DOI: 10.1016/j.jmst.2021.04.024
9. Hao, X., Dong, H., Li, P., and Xia, Y. 2019. Dissimilar joining of TC4 alloy to ST16 steel by GTAW. *Journal of Manufacturing Processes* 37: 413–417. DOI: 10.1016/j.jmapro.2018.12.016
10. Li, C., Si, X., Bian, S., Dong, Z., Huang, Y., Qi, J., and Feng, J. 2020. Diffusion bonding of Ti and Zr at ultra-low temperature via surface nano-crystallization treatment. *Materials Science & Engineering A* 785: 139413. DOI: 10.1016/j.msea.2020.139413
11. Lin, J., Yang, Z., Wei, H., Wang, Y., Ma, Z., and Wang, D. 2018. An investigation on diffusion bonding of TZM alloy and Nb-Zr alloy using Ni foil as an interlayer. *Journal of Alloys and Compounds* 743: 780–788. DOI: 10.1016/j.jallcom.2018.01.162

12. Aboudi, D., Lebaili, S., Taouinet, M., and Zollinger, J. 2017. Microstructure evolution of diffusion welded 304L/Zircaloy<sub>4</sub> with copper interlayer. *Materials & Design* 116: 386–394. DOI: 10.1016/j.matdes.2016.12.008
13. Li, P., Wang, S., Xia, Y., Hao, X., and Dong, H. 2020. Diffusion bonding of AlCoCrFeNi<sub>2.1</sub> eutectic high entropy alloy to TiAl alloy. *Journal of Materials Science & Technology* 45: 59–69. DOI: 10.1016/j.jmst.2019.10.041
14. Alhazaa, A., and Khan, T. 2010. Diffusion bonding of Al7075 to Ti-6Al-4V using Cu coatings and Sn-3.6Ag-1Cu interlayers. *Journal of Alloys and Compounds* 494(1–2): 351–358. DOI: 10.1016/j.jallcom.2010.01.037
15. Yao, T., Du, K., Wang, H., Huang, Z., Li, C., Li, L., Hao, Y., Yang, R., and Ye, H. 2017. In situ scanning and transmission electron microscopy investigation on plastic deformation in a metastable beta titanium alloy. *Acta Materialia* 133: 21–29. DOI: 10.1016/j.actamat.2017.05.018
16. Lai, M., Li, T., and Raabe, D. 2018.  $\omega$  phase acts as a switch between dislocation channeling and joint twinning- and transformation-induced plasticity in a metastable  $\beta$  titanium alloy. *Acta Materialia* 151: 67–77. DOI: 10.1016/j.actamat.2018.03.053
17. Dong, K., and Kong, J. 2019. A high-strength vacuum-brazed TiAl/Ni joint at room temperature and high temperature with an amorphous foil Zr-Al-Ni-Co filler metal. *Journal of Manufacturing Processes* 44: 389–396. DOI: 10.1016/j.jmapro.2019.05.024
18. Martínez, V., Aguilar, C., Marín, J., Ordoñez, S., and Castro, F. 2007. Mechanical alloying of Cu-Mo powder mixtures and thermodynamic study of solubility. *Materials Letters* 61(4–5): 929–933. DOI: 10.1016/j.matlet.2006.11.070
19. Ning, J., Zhang, L., Zhang, L., Long, J., and Na, S. 2020. Effects of power modulation on behaviours of molten pool and keyhole during laser-arc hybrid welding of pure copper. *Materials & Design* 194: 108829. DOI: 10.1016/j.matdes.2020.108829
20. Aydin, K., Kaya, Y., and Kahraman, N. 2012. Experimental study of diffusion welding/bonding of titanium to copper. *Materials & Design* 37: 356–368. DOI: 10.1016/j.matdes.2012.01.026
21. Song, M., Zhao, X., Guo, W., Feng, J., and Huang, D. 2007. Diffusion bonding of Ti-6Al-4V to ZQSn10-10 in vacuum. *China Welding* 16(1): 1–5.
22. Shen, Q., Xiang, H., Luo, G., Su, X., and Zhang, L. 2013. Interfacial microstructure and mechanical properties of diffusion bonded TC4/OCr18Ni9/oxygen free copper joints. *Materials & Design* 50: 230–234. DOI: 10.1016/j.matdes.2013.01.042
23. Shen, Q., Xiang, H., Li, M., Luo, G., Wang, Y., Wang, C., and Zhang, L. 2015. Low temperature diffusion bonding of Ti-6Al-4V to oxygen free copper with high bonding strength using pure Ag interlayer. *Rare Metal Materials and Engineering* 44: 2607–2611. DOI: 10.1016/j.matdes.2013.01.042
24. Zhao, H., Feng, J., Song, M., and Zhao, X. 2008. Study of diffusion bonding of Ti-6Al-4V and ZQSn10-10 with metal interlayer. *China Welding* 17(1): 36–39.
25. Collins, P., Banerjee, R., Banerjee, S., and Fraser, H. 2003. Laser deposition of compositionally graded titanium-vanadium and titanium-molybdenum alloys. *Materials Science & Engineering A* 352(1–2): 118–128. DOI: 10.1016/s0921-5093(02)00909-7
26. Liu, Y., Luo, Y., Zhao, D., Zhang, G., and Kang, L. 2017. Interfacial behavior and joint performance of high-entropy alloy CoCrFeMnNi and pure Cu joints obtained by vacuum diffusion welding. *Journal of Mechanical Engineering* 53(2): 84–91. DOI: 10.3901/JME.2017.02.084
27. Wu, B., Dong, H., Li, P., Ma, Y., Yang, Y., Zou, C., and Li, C. 2022. Vacuum diffusion bonding of TC4 titanium alloy and T2 copper by a slow cooling heat treatment. *Journal of Materials Processing Technology* 305: 117595. DOI: 10.1016/j.jmatprotec.2022.117595
28. Li, P., Li, C., Dong, H., Wu, B., Ma, Y., Zou, C., and Yang, Y. 2022. Vacuum diffusion bonding of TC4 titanium alloy to 316L stainless steel with AlCoCrCuNi<sub>2</sub> high-entropy alloy interlayer. *Journal of Alloys and Compounds* 909: 164698. DOI: 10.1016/j.jallcom.2022.164698
29. Huang, L., Cui, Y., Chang, H., Zhong, H., Li, J., and Zhou, L. 2010. Assessment of atomic mobilities for bcc phase of Ti-Al-V system. *Journal of Phase Equilibria and Diffusion* 31(2): 135–143. DOI: 10.1007/s11669-009-9641-8
30. Takeuchi, A., and Inoue, A. 2005. Classification of bulk metallic glasses by atomic size difference, heat of mixing and period of constituent elements and its application to characterization of the main alloying element. *Materials Transactions* 46(12): 2817–2829. DOI: 10.2320/matertrans.46.2817
31. Zhang, M., and Kelly, P. 2005. Edge-to-edge matching and its applications: Part I. Application to the simple HCP/BCC system. *Acta Materialia* 53(4): 1073–1084. DOI: 10.1016/j.actamat.2004.11.007
32. Zheng, L., Li, F., and Zhou, Y. 2012. Preparation, microstructure, and mechanical properties of TiB<sub>2</sub> using Ti<sub>3</sub>AlC<sub>2</sub> as a sintering aid. *Journal of the American Ceramic Society* 95: 2028–2034. DOI: 10.1111/j.1551-2916.2012.05204.x
33. Lappalainen, R. 1985. Diffusion of aluminum in polycrystalline vanadium. *Nuclear Instruments and Methods in Physics Research Section B: Beam Interactions with Materials and Atoms* 7: 44–48. DOI: 10.1016/0168-583X(85)90527-0
34. Bakker, H., Bonzel, H. P., Bruff, C. M., Dayananda, M. A., Gust, W., Horvath, J., Kaur, I., Kidson, G. V., LeClaire, A. D., Mehrer, H., Murch, G. E., Neumann, G., Stolica, N., and Stolwijk, N. A. 1990. Diffusion in solid metals and alloys. *Landolt-Börnstein — Group III Condensed Matter* 26: 306–307. DOI: 10.4028/www.scientific.net/DDF.4.296
35. Velmurugan, C., Senthilkumar, V., Sarala, S., and Arivarasan, J. 2016. Low temperature diffusion bonding of Ti-6Al-4V and duplex stainless steel. *Journal of Materials Processing Technology* 234: 272–279. DOI: 10.1016/j.jmatprotec.2016.03.013

36. Xia, Y., Dong, H., and Li, P. 2020. Brazing TC4 titanium alloy/316L stainless steel joint with  $Ti_{50-x}Zr_xCu_{39}Ni_{11}$  amorphous filler metals. *Journal of Alloys and Compounds* 849: 156650. DOI: 10.1016/j.jallcom.2020.156650

37. Su, X., Luo, G., Shen, Q., Zeng, H., Wang, C., and Zhang, L. 2010. Study on diffusion welding of TC4/OFC in vacuum. *Rare Metal Materials and Engineering* 39: 2044–2047.

38. Zhao, H., Zhao, H., Song, M., Zhao, X., and Feng, J. 2008. Influence of different transition metals on properties of diffusion bonding joint of TC4/ZQSn10-10. *Materials for Mechanical Engineering* 7: 38–40.

39. Guo, W., Zhao, X., Song, M., Feng, J., and Yang, B. 2006. Diffusion bonding of Ti-6Al-4V to QAl 10-3-1.5 with Ni/Cu interlayers. *Journal of Materials Science & Technology* 22(6): 101–104.

40. Cao, R., Feng, Z., and Chen, J. 2014. Microstructures and properties of titanium-copper lap welded joints by cold metal transfer technology. *Materials & Design* 53: 192–201. DOI: 10.1016/j.matdes.2013.06.030

41. Orhan, N., Aksoy, M., and Eroglu, M. 1999. A new model for diffusion bonding and its application to duplex alloys. *Materials Science & Engineering A* 271(1–2): 458–468. DOI: 10.1016/S0921-5093(99)00315-9

**BAOSHENG WU, HONGGANG DONG** ([donghg@dlut.edu.cn](mailto:donghg@dlut.edu.cn)), **YUETING MA, PENG LI, CHAO LI, LIBING HUANG**, and **LIANGLIANG ZHANG** are with the School of Materials Science and Engineering, Dalian University of Technology, Dalian, China.



## Can We Talk?

The *Welding Journal* staff encourages an exchange of ideas with you, our readers. If you'd like to ask a question, share an idea, or voice an opinion, you can call, write, or email. Staff email addresses are listed below, along with a guide to help you interact with the right person.

### Publisher/Editor

Annette Alonso, [aalonso@aws.org](mailto:aalonso@aws.org), ext. 299  
General Management, Reprint Permission,  
Copyright Issues, Editorial Content

### Managing Editor

Kristin Campbell, [kcampbell@aws.org](mailto:kcampbell@aws.org), ext. 257  
Feature Articles

### Sr. Editor

Cindy Wehl, [cwehl@aws.org](mailto:cwehl@aws.org), ext. 256  
Section News, *SPRAYTIME*®

### Associate Editors

Alexandra Quiñones, [aquinones@aws.org](mailto:aquinones@aws.org), ext. 465  
Arc-Tist Corner, Industry News  
Katie Pacheco, [kpacheco@aws.org](mailto:kpacheco@aws.org), ext. 275  
Society News, New Products

### Education Editor

Roline Pascal, [rpascal@aws.org](mailto:rpascal@aws.org), ext. 303  
Coming Events, Personnel

### Managing Editor, Digital and Design; Editor of *Inspection Trends and Welding Journal en Español*

Carlos Guzman, [cguzman@aws.org](mailto:cguzman@aws.org), ext. 348  
Inspection and Spanish-Language Content,  
Design and Production

### Production Manager

Zaida Chavez, [zaida@aws.org](mailto:zaida@aws.org), ext. 265  
Design and Production

### Assistant Production Manager

Brenda Flores, [bflores@aws.org](mailto:bflores@aws.org), ext. 330  
Design and Production, Peer Review Coordinator

### Advertising

Scott Beller, [sbeller@aws.org](mailto:sbeller@aws.org), ext. 319  
Lea Owen, [lea@aws.org](mailto:lea@aws.org), ext. 220

### Subscriptions

Giovanni Valdes, [gvaldes@aws.org](mailto:gvaldes@aws.org), ext. 329